

# Long-term tidal evolution of short-period planets with companions

Rosemary A. Mardling<sup>1\*</sup>

<sup>1</sup>*School of Mathematical Sciences, Monash University, Victoria, 3800, Australia*

Accepted ... Received ...; in original form ...

## ABSTRACT

Of the fourteen transiting extrasolar planetary systems for which radii have been measured, at least three appear to be considerably larger than theoretical estimates suggest. It has been proposed by Bodenheimer, Lin & Mardling that undetected companions acting to excite the orbital eccentricity are responsible for these oversized planets, as they find new equilibrium radii in response to being tidally heated. In the case of HD 209458, this hypothesis has been rejected by some authors because there is no sign of such a companion at the  $5 \text{ ms}^{-1}$  level, and because it is difficult to say conclusively that the eccentricity is non-zero. Transit timing analysis as well as a direct transit search have further constrained the existence of very short-period companions, especially in resonant orbits. Whether or not a companion is responsible for the large radius of HD 209458b, almost certainly some short-period systems have companions which force their eccentricities to nonzero values. This paper is dedicated to quantifying this effect.

The eccentricity of a short-period planet will only be excited as long as its (non-resonant) companion's eccentricity is non-zero. Here we show that the latter decays on a timescale which depends on the structure of the *interior* planet, a timescale which is often shorter than the lifetime of the system. *This includes Earth-mass planets in the habitable zones of some stars.* We determine which configurations are capable of sustaining significant eccentricity for at least the age of the system, and show that these include systems with companion masses as low as a fraction of an Earth mass. The orbital parameters of such companions are consistent with recent calculations which show that the migration process can induce the formation of low mass planets external to the orbits of hot Jupiters. Systems with inflated planets are therefore good targets in the search for terrestrial planets.

**Key words:** planetary systems – celestial mechanics – stellar dynamics – methods: analytical – planetary systems: formation

## 1 INTRODUCTION

While most extrasolar planet discoveries to date have relied on the radial velocity method of detection with its inherent uncertainty in the planetary mass, a few systems have been observed in transit, thereby breaking this degeneracy. Not only does this allow a reasonably accurate determination of the planetary mass (given a reliable estimate for the stellar mass is available), it allows one to estimate the radius of the planet, and hence its density. Before the discovery that HD 209458b transited its host star (Charbonneau et al. 2000; Henry et al. 2000), it was by no means clear that the planets discovered till then, all with masses similar to or more than Jupiter's, were gas giants. The extra information gleaned from photometric transit data has provided the opportunity to study planetary *structure* (Bodenheimer, Lin & Mardling 2001), while spectroscopic data have revealed their chemical composition (Charbonneau et al. 2002). In the former case, determination of the planetary radius

\* E-mail: mardling@sci.monash.edu.au

**Table 1.** Observational data for inflated planets

Planet	Period (day)	$m_*$ ( $M_\odot$ )	$m_p$ ( $M_J$ )	$a_p$ (AU)	$e_p^{obs}$	$R_p$ ( $R_J$ )
HD 209458b	3.5247	1.10	$0.64 \pm 0.06$	0.045	$0.014 \pm 0.009^a$	$1.32 \pm 0.03$
WASP-1b <sup>b</sup>	2.5199	1.15	$0.79^{+0.13}_{-0.06}$	0.0379	-	$1.443 \pm 0.039$
HAT-P-1b	4.4653	1.12	$0.53 \pm 0.04$	0.0551	$0.09 \pm 0.02^c$	$1.36^{+0.11}_{-0.09}$

<sup>a</sup> Laughlin et al. (2005a).<sup>b</sup> Stempels et al. (2007).<sup>c</sup> This value is based on very little data (Bakos et al. 2006).

allows one to put constraints on the possible existence of a planetary core, and this in turn allows one to constrain the mode of planet formation, at least for that planet. In principle this allows a choice between the core accretion model (Safronov 1969; Wetherill 1980; Bodenheimer & Pollack 1986) and the gravitational instability model (Kuiper 1951; Cameron 1978; Boss 1997), although it is not clear that the latter should produce core-less planets given accretion of solids plus subsequent gravitational settling almost certainly follows formation. Either way, such an exercise requires knowledge of the equilibrium structure of a gas giant planet, with and without a core, and with and without external and internal heating.

While it can be argued that there are problems matching theoretical radii with observation for *all* transiting planets (Burrows et al. 2007), three stand out as particularly excessive. These are HD 209458b (Charbonneau et al. 2000; Henry et al. 2000; Knutson et al. 2007), WASP-1b (Collier Cameron et al. 2006) and HAT-P-1b (Bakos et al. 2006), for which the planetary radii and other observationally derived parameters are listed in Table 1. Data for HD 209458 and HAT-P-1 are taken from Burrows et al. (2006) and references therein, except for the eccentricities, while data for WASP-1 are taken from Stempels et al. (2007). Here  $m_*$  and  $m_p$  are the masses of the star and planet respectively,  $a_p$  and  $e_p$  are the orbital semimajor axis and eccentricity and  $R_p$  is the estimated planetary radius ( $R_J$  is Jupiter’s radius). The eccentricity of HD 209458b is from Laughlin et al. (2005a), a paper devoted specifically to discussing this contentious orbital element, while that of HAT-P-1b is from Bakos et al. (2006), a value based on very little data. However, as pointed out by the latter authors, HAT-P-1b is further from its parent star than HD 209458b, and is such that the relatively large estimated value of 0.09 produces a similar planetary radius.

Various mechanisms have been suggested to account for the excess radii of the planets listed in Table 1. Obvious contenders are stellar irradiation (Burrows et al. 2000; Guillot & Showman 2002; Bodenheimer, Laughlin & Lin 2003; Burrows, Sudarsky & Hubbard 2003; Arras & Bildsten 2006; Fortney, Marley & Barnes 2007; Burrows et al. 2007) and tidal forcing by a companion planet (Bodenheimer, Lin & Mardling 2001; Bodenheimer, Laughlin & Lin 2003), the latter requiring non-zero eccentricity of the observed planetary orbit to be viable. A less obvious mechanism has been proposed by Winn & Holman (2005) in which “obliquity tides” are forced if the system can manage to remain in a suitable Cassini state. Fabrycky, Johnson & Goodman (2007) verify that in principle it is possible for this mechanism to operate, however, they show that the system cannot dissipate energy rapidly enough for it to make a structural difference to the planet.

This paper focuses on the mechanism of tidal forcing provided by a companion planet, and hence requires that the orbit of the transiting planet be non-circular. Using a bootstrap Monte Carlo technique to estimate confidence intervals for the eccentricity of HD 209458b, Laughlin et al. (2005a) find that  $e_p < 0.049$  with 99.73% confidence,  $e_p < 0.034$  with 95.4% confidence, and  $e_p < 0.02$  with 68.3% confidence, with longitude of periastron  $\varpi_p = 80^\circ \pm 80^\circ$ . Their best-fit measurement for the eccentricity is  $e_p = 0.014$ . However, they point out that because  $e_p$  has a hard lower bound of zero, any best-fit model to a radial velocity data set will have  $e_p \geq 0$ , with largest estimates corresponding to  $\varpi_p \simeq 90^\circ$  and  $270^\circ$ . Using synthetic data corresponding to a truly circular orbit, such bootstrap trials produce a distribution in  $\varpi_p - e_p$  space which is symmetric about these two values, while use of the real radial velocity data produces a distinctly asymmetric distribution which is biased towards  $\varpi_p = 90^\circ$ . This suggests that in fact  $e_p \neq 0$ , although  $e_p = 0$  cannot be ruled out. Laughlin et al. (2005a) point out that the fact that the estimate for  $\varpi_p$  is centred near  $90^\circ$  suggests that even if HD 209458b has a non-zero eccentricity, timing of the secondary eclipse will find  $e_p \cos \varpi_p \simeq 0$ , as has recently been found by Deming et al. (2005) in the infrared. Note also that the orbital model of Laughlin et al. (2005a) leads to a stellar jitter estimate of  $3.3 \text{ m s}^{-1}$  which is close to the predicted value of  $2.8 \text{ m s}^{-1}$ . Thus, at least for HD 209458, we concentrate our attention in this paper on companions which produce stellar reflex velocities not much larger than this value.

The presence of a very short-period companion to HD 209458b has been ruled out by transit-timing analysis for interior and exterior planets with periods up to 21 days (corresponding to the 6:1 resonance at 0.16 AU) (Agol & Steffen 2007), as well as by a direct transit search for planets with radii down to  $2R_\oplus$  and periods up to 14 days (Croll et al. 2007). Here we will concentrate on companion planets with semimajor axes greater than these lower bounds.

This paper presents a generic analysis for short-period systems with external companion planets (low-mass or otherwise), estimating the range of orbital parameters and masses required for such companions to be responsible for inflated radii. An

unexpected result is that very low mass planets are sometimes capable of inducing significant tidal forcing on extremely long timescales. Section 2 discusses the relationship between the eccentricity and the  $Q$ -value of a planet for a given value of the planet's luminosity, the  $Q$ -value or tidal quality factor (Goldreich & Soter 1966) being a measure of how efficiently the tides dissipate their oscillation energy. Section 3 discusses three-body dynamics in the presence of dissipation (see also Murray & Dermott (2000) and Adams & Laughlin (2006b)). We start by reviewing the secular evolution of point-mass coplanar three-body systems, with and without relativistic effects, deriving explicit formulae for the periods of variation of the eccentricities and their amplitudes. We identify the orbital parameters which correspond to libration and circulation of the angle  $\eta \equiv \varpi_p - \varpi_c$ , where  $\varpi_c$  is the longitude of periastron of the companion, and in particular find the fixed points in  $e_p - \eta$  space. We then show that tidal damping results in the system evolving towards the relevant fixed point (now a *quasi*-fixed point) on three times the tidal damping timescale. Once this is achieved the system continues to evolve toward the true fixed point for which both eccentricities are zero. The timescale for this latter phase may be several orders of magnitude longer than the tidal damping timescale, and can in fact be much longer than the age of the system. We illustrate the theory for hypothetical companions to HD 209458, and show that companion masses as low as a fraction of an Earth mass are capable of sustaining non-zero eccentricities in the observed planetary orbit for at least the age of the system, and in some cases at the level required to sustain the observed radii at the current epoch.

Section 4 maps out regions in  $m_c - a_c$  parameter space, where  $m_c$  and  $a_c$  are the mass and semimajor axis of a hypothetical companion, for which the eccentricities of HD 209458b and HAT-P1b would be at their observed level, as well as for WASP-1b which for which the eccentricity is currently unconstrained. Section 5 applies the secular theory developed here to determine which configurations have circularized companion planets, while Section 6 presents a summary and a discussion.

## 2 THE ECCENTRICITY-RADIUS RELATION

Various authors have studied the problem of the response of a planet to internal and external heat sources (eg. Burrows et al. 2000, Bodenheimer, Lin & Mardling 2001, Bodenheimer, Laughlin & Lin 2003, Burrows et al. 2007). In particular, models include planets with and without cores, with and without stellar irradiation, and with and without an internal heat source. In all these models the planet assumes an equilibrium radius,  $R_p$ , and it is the relationship between this and the rate of energy dissipation in the planet,  $\mathcal{L}_p$ , that is used in an attempt to explain the range of planetary radii observed in transiting planets.

In the case that  $\mathcal{L}_p$  is due to tides raised by an external companion, the rate of internal energy dissipation in the planet is given by (eg., Yoder & Peale (1981), Bodenheimer, Laughlin & Lin (2003))

$$\dot{E}_d = \left( \frac{Gm_*m_p}{a_p} \right) \left( \frac{e_p^2}{\tau_{circ}} \right), \quad (1)$$

where

$$\tau_{circ} \equiv \frac{e_p}{\dot{e}_p} = \frac{2}{21n_p} \left( \frac{Q_p}{k_p} \right) \left( \frac{m_p}{m_*} \right) \left( \frac{a_p}{R_p} \right)^5 \quad (2)$$

is the circularization timescale of the orbit, with  $n_p$  the orbital frequency,  $k_p$  the tidal Love number of the planet and  $Q_p$  its  $Q$ -value or tidal quality factor (Goldreich & Soter 1966).<sup>1</sup> Equating this to the power,  $\mathcal{L}_p$ , needed to maintain an observed planetary radius gives  $e_p$  in terms of the observable quantities  $m_*$ ,  $R_p$  and  $a_p$  ( $m_p$  actually drops out), as well as the theoretical quantities  $Q_p$ ,  $k_p$  and  $\mathcal{L}_p$ :

$$e_p = 0.020 \left( \frac{m_*}{M_\odot} \right)^{-5/4} \left( \frac{R_p}{R_J} \right)^{-5/2} \left( \frac{a_p}{0.04 \text{ AU}} \right)^{15/4} \left( \frac{Q_p}{10^5} \right)^{1/2} \left( \frac{k_p}{k_J} \right)^{-1/2} \left( \frac{\mathcal{L}_p}{10^{-8} L_\odot} \right)^{1/2}, \quad (3)$$

where  $k_J = 0.34$  is the tidal Love number for Jupiter. Burrows et al. (2007) calculate  $\mathcal{L}_p$  for *coreless solar metallicity planets which are irradiated by their parent stars*, values for which are listed in Table 2 under  $\mathcal{L}_p^{Bu}$ . Bodenheimer, Laughlin & Lin (2003) calculate  $\mathcal{L}_p$  specifically for HD 209458b only (in addition to various generic models), and find a value for  $\mathcal{L}_p$  ten times higher for a coreless planet, while for a planet with a  $20 M_\oplus$  core, they find  $\mathcal{L}_p$  is *another* factor of ten higher. Note that they take a slightly higher value for  $R_p$  ( $1.35 R_J$ ). Values for  $e_p$  corresponding to  $\mathcal{L}_p = \mathcal{L}_p^{Bu}$  and  $Q_p = 10^5$  (see discussion below) are shown in Table 2 as well as values corresponding to  $\mathcal{L}_p = 10 \mathcal{L}_p^{Bu}$ . The estimated value of  $e_p$  for HD 209458b (listed under  $e_p^{obs}$ ) is more consistent with  $\mathcal{L}_p = \mathcal{L}_p^{Bu}$  than  $\mathcal{L}_p = 10 \mathcal{L}_p^{Bu}$  while the opposite is true for HAT-P-1b, although the eccentricity value for the latter awaits refinement. Note that in reality  $\mathcal{L}_p$  is a function of  $R_p$  and  $m_p$ , however, its role in equation (3) is to parameterize various authors' models.

<sup>1</sup> Note that Goldreich & Soter (1966) use a modified  $Q$ -value,  $Q'_p$ , which absorbs the Love number such that  $Q'_p = 3Q_p/2k_p$ ; equation (4) in (Bodenheimer, Laughlin & Lin 2003) should have  $Q'_p$  instead of  $Q_p$ . Another potential source of confusion is the use of the (quadrupole) apsidal motion constant  $k_2$  rather than the tidal Love number; these are related by  $k_p = 2k_2$ .

**Table 2.** Theoretical data assuming  $Q_p = 10^5$ 

Planet	Age (Gyr)	$\tau_{circ}$ (Gyr)	$\mathcal{L}_p^{Bu}$ ( $L_\odot$ )	$e_p(\mathcal{L}_p^{Bu})$	$e_p(10 \mathcal{L}_p^{Bu})$	$e_p^{obs}$
HD 209458b	$5.5 \pm 1.5^a$	0.045	$1.02 \times 10^{-8}$	0.014	0.046	$0.014 \pm 0.009$
WASP-1b	$2.0 \pm 1.0^b$	0.011	$4.49 \times 10^{-8}$	0.012	0.037	-
HAT-P-1b	$3.6 \pm 1.0^a$	0.109	$1.32 \times 10^{-8}$	0.031	0.098	$0.09 \pm 0.02$

<sup>a</sup> Burrows et al. (2007)<sup>b</sup> Stempels et al. (2007)

In both the models of Burrows et al. (2007) and Bodenheimer, Laughlin & Lin (2003), tidal energy is deposited homogeneously throughout the planet’s envelope and dissipated locally. If, for example, tidal energy is predominantly dissipated in the *outer layers* of the planet, a significantly smaller value of  $\mathcal{L}_p$ , and hence  $e_p$ , may be required to achieve the same planetary radius (as long as the energy is dissipated sufficiently deep below the surface; Wu (2005) finds that tidal excitation of inertial modes results in energy being dissipated very close to the surface resulting in very little structural adjustment). Alternatively, for a given  $e_p$  one would require larger values of  $Q_p$  for correspondingly smaller values of  $\mathcal{L}_p$ . Note that this scenario makes it difficult to draw conclusions about the existence or otherwise of a planetary core.

There is significant uncertainty in the theory of tidal damping in stars and planets, much of it associated with internal structure and (in the case of gaseous objects) the theory of turbulent dissipation (see Ogilvie & Lin (2004) for an excellent review). In the case of solid planets, one can infer damping timescales based on laboratory measurements of  $Q$ -values of solid materials, and for the special case of the Earth-Moon system, one can actually measure the rate of recession of the Moon. In the case of Jupiter and its satellite system, it is possible to put lower and upper bounds on Jupiter’s  $Q$ -value ( $6 \times 10^4 - 2 \times 10^6$ : Yoder & Peale 1981). These bounds are inferred from the existence of the Laplace resonance: if  $Q_J$  were too low Io would have already passed through the 2:1 resonance with Europa (probably destabilizing the system), while if it were too high it would never have been captured in the first place. Similarly for Uranus,  $Q_U < 39,000$  (Tittlemore & Wisdom 1989) while for Neptune,  $12,000 < Q_N < 330,000$  (Banfield & Murray 1992).

There are various factors which might be expected to influence the  $Q$ -value of a hot Jupiter and how this might differ from that of Jupiter. One obvious difference between hot Jupiters and our own Jupiter are spin rates. While Jupiter’s spin period is 10 hrs, hot Jupiters are synchronous with the orbital motion and hence have periods around an order of magnitude longer. Goldreich & Soter (1966, p388) point out that the smaller the mass of a planet, the lower the  $Q$ -value. More recent work by Ogilvie & Lin (2004) and Wu (2005) who consider tidal forcing in slowly rotating planets (appropriate to synchronously rotating short-period planets) find that  $Q$ -values for such planets tend to be similar to that of Jupiter. Wu (2003) shows that the observed orbital parameters of short-period extrasolar planets indicate that their  $Q$ -values lie between  $3 \times 10^4$  and  $3 \times 10^5$ . The lower value is increased if one takes into account the fact that planets are likely to arrive at their current positions with significantly larger radii than those observed today (see Fig. 1 of Bodenheimer, Lin & Mardling (2001)). Throughout this paper we use mostly  $Q_p = 10^5$  to illustrate the theory developed here.

### 3 LONG-TERM ECCENTRICITY EVOLUTION

The estimated ages of HD 209459, HAT-P-1 and WASP-1 are shown in Table 2 together with the circularization timescales of their planets (assuming  $Q_p = 10^5$ ). Clearly a mechanism is needed to maintain orbital eccentricity if tidal heating is the source of energy which maintains the inflated planetary radii. It seems to be implicitly assumed that the oscillatory secular variations in the eccentricities of a pair of close planets (Murray & Dermott 2000) prevail indefinitely, even in the presence of tidal dissipation. In this section we show that the natural endpoint of such evolution is in fact a pair of circular orbits, with the structural properties of the tidally forced planet determining (at least in part) the timescale on which this occurs. This evolution occurs in three stages (see Figure 3): (1) circulation of the angle between the lines of apsides of the two planets accompanied by the slow oscillation of the eccentricities at constant amplitude, together with decline of the *mean* value of the inner planet’s eccentricity until it reaches a (quasi)-fixed value: this occurs on the circularization timescale; (2) libration of the angle between the lines of apsides accompanied by the slow oscillation of the eccentricities with reducing amplitude but maintenance of the mean value of the inner eccentricity: this occurs on *twice* the circularization timescale; and (3) either (a): a slow non-oscillatory decline in both eccentricities to zero or (b): maintenance of the inner eccentricity for some (often extremely long) period of time followed by its *increase* to some maximum value followed by an often fast decline of both eccentricities to zero. Whether or not the final phase occurs via route (a) or (b), it proceeds on a timescale sometimes several orders of magnitude longer than the circularization timescale.

In general, the rates of change of a planet’s orbital elements will have contributions from companions if they exist, the

relativistic post-Newtonian contribution to the potential of the star, the tidal and spin bulges of the star and planet, and tidal dissipation in the atmospheres of the star and the planet (Mardling & Lin 2002; Adams & Laughlin 2006a,b). For coplanar systems, planetary elements which evolve are the semimajor axis, the eccentricity and the longitude of periastron. The only effect which contributes to a change in the semimajor axis (except when the system is in a resonance) is tidal dissipation, while for short-period systems the apsidal motion is dominated by the third body and the relativistic potential of the star. The eccentricity in turn is dominated by the third body and tidal damping. We will assume that the orbits are coplanar, that the planet is synchronously rotating with the orbital motion, and that the spin bulge of the star is negligible. For the analysis we will assume that the rate of change of the planet's semimajor axis is negligible, while numerical integrations will include this effect (see Rasio et al. (1996) and Mardling & Lin (2004) for discussions of this point).

The plan of this section is as follows: (1) Study the equations governing the secular evolution of three coplanar Newtonian point masses for which  $e_p$  is small compared to the companion eccentricity and  $m_p \ll m_*$ , and determine the regions of parameter space for which the system librates or circulates. In particular, determine the fixed points of this dynamical system; (2) Determine how the results of (1) are modified by the inclusion of post-Newtonian terms in the potential of the star; (3) Introduce tidal damping and show that the system evolves towards doubly circular orbits on timescales described above.

### 3.1 Newtonian three-body secular evolution

Consider a *coplanar* point-mass three-body system with masses  $m_*$ ,  $m_p$  and  $m_c$  (for star, planet and companion respectively) for which  $m_p \ll m_*$ , but with no constraints on  $m_c$ , and let the star-planet and star-companion semimajor axes be  $a_p$  and  $a_c$  respectively.<sup>2</sup> Further, let the corresponding eccentricities be  $e_p$  and  $e_c$ , with  $e_p \ll 1$  but again with no constraint on  $e_c$ , and let the longitudes of periastra be  $\varpi_p$  and  $\varpi_c$ . While no energy is exchanged between the orbits of a (nonresonant) stable system (and hence the semimajor axes remain constant), to first order in  $e_p$  the orbit-averaged rates of change of  $e_p$ ,  $e_c$ ,  $\varpi_p$  and  $\varpi_c$  are (see Mardling (2007a) for the full secular equations to all orders and including inclination and precession)

$$\frac{de_p}{dt} = -\frac{15}{16} n_p e_c \left(\frac{m_c}{m_*}\right) \left(\frac{a_p}{a_c}\right)^4 \frac{\sin(\varpi_p - \varpi_c)}{(1 - e_c^2)^{5/2}}, \quad (4)$$

$$\frac{de_c}{dt} = \frac{15}{16} n_c e_p \left(\frac{m_p}{m_*}\right) \left(\frac{a_p}{a_c}\right)^3 \frac{\sin(\varpi_p - \varpi_c)}{(1 - e_c^2)^2}, \quad (5)$$

$$\frac{d\varpi_p}{dt} = \frac{3}{4} n_p \left(\frac{m_c}{m_*}\right) \left(\frac{a_p}{a_c}\right)^3 (1 - e_c)^{-3/2} \left[ 1 - \frac{5}{4} \left(\frac{a_p}{a_c}\right) \left(\frac{e_c}{e_p}\right) \frac{\cos(\varpi_p - \varpi_c)}{1 - e_c^2} \right] \quad (6)$$

and

$$\frac{d\varpi_c}{dt} = \frac{3}{4} n_c \left(\frac{m_p}{m_*}\right) \left(\frac{a_p}{a_c}\right)^2 (1 - e_c^2)^{-2} \left[ 1 - \frac{5}{4} \left(\frac{a_p}{a_c}\right) \left(\frac{e_p}{e_c}\right) \frac{(1 + 4e_c^2)}{(1 - e_c^2)} \cos(\varpi_p - \varpi_c) \right]. \quad (7)$$

where  $n_p$  and  $n_c$  are the orbital frequencies (mean motions) of the planet and companion respectively. Note that Mardling & Lin (2002) and Mardling (2007a) employ a Legendre expansion in the ratio  $a_p/a_c$  to derive the rates of change of the elements and make no assumptions about the mass ratios, eccentricities or inclinations, in contrast to the *literal* expansion used by Murray & Dermott (2000) which relies on the smallness of the eccentricities and inclinations but holds for all semimajor axes ratios. Equations (4) to (7) are given to *octopole* order; see also Lee & Peale (2003) and Ford & Rasio (2000).

#### 3.1.1 Libration versus Circulation of $\varpi_p - \varpi_c$

In order to derive simple conditions under which the angle  $\varpi_p - \varpi_c$  circulates or librates, we assume that  $e_c$  is significantly greater than  $e_p \ll 1$  (a situation relevant to the present study; see Nagasawa, Lin & Ida (2003) for an alternative treatment). Then  $\dot{e}_c \simeq 0$  and we can write

$$\dot{e}_p = -W_o e_c \sin \eta \quad (8)$$

and

$$\dot{\eta} = W_q - W_o \left(\frac{e_c}{e_p}\right) \cos \eta, \quad (9)$$

where  $\eta \equiv \varpi_p - \varpi_c$  and  $W_q$  and  $W_o$  are constants ( $q$  for quadrupole and  $o$  for octopole) defined by

<sup>2</sup> In fact, a Jacobian coordinate system is used to derive equations (4) to (7) so that the companion's orbital elements are actually measured with respect to the centre of mass of the star-planet system.

$$W_q = \frac{3}{4} n_p \left( \frac{a_p}{a_c} \right)^3 \left( \frac{m_c}{m_*} \right) \varepsilon_c^{-3} \left[ 1 - \sqrt{\frac{a_p}{a_c}} \left( \frac{m_p}{m_c} \right) \varepsilon_c^{-1} \right] \quad (10)$$

and

$$W_o = \frac{15}{16} n_p \left( \frac{a_p}{a_c} \right)^4 \left( \frac{m_c}{m_*} \right) \varepsilon_c^{-5}, \quad (11)$$

where  $\varepsilon_c = \sqrt{1 - e_c^2}$ . The fixed points of (8) and (9) are

$$(e_p, \eta) = (e_c W_o / W_q, 2n\pi) \text{ when } W_q > 0, \quad (12)$$

and

$$(e_p, \eta) = (-e_c W_o / W_q, (2n+1)\pi) \text{ when } W_q < 0. \quad (13)$$

Here  $n$  is any integer. Writing  $x \equiv e_p - e_p^{(eq)}$ , where

$$e_p^{(eq)} = e_c W_o / |W_q| = \frac{(5/4)(a_p/a_c) e_c \varepsilon_c^{-2}}{\left| 1 - \sqrt{a_p/a_c} (m_p/m_c) \varepsilon_c^{-1} \right|}, \quad (14)$$

and linearizing about  $\eta = 0$  we have

$$\dot{x} = -e_c W_o \eta, \quad \dot{\eta} = \left( \frac{W_q^2}{W_o} \right) \frac{x}{e_c}, \quad (15)$$

or

$$\ddot{\eta} + W_q^2 \eta = 0 \quad (16)$$

which has solutions

$$\eta(t) = A \cos(W_q t + \beta), \quad (17)$$

where

$$A^2 = \eta(0)^2 + \left( 1 - e_p(0)/e_p^{(eq)} \right)^2 \quad \text{and} \quad \tan \beta = \left( 1 - e_p(0)/e_p^{(eq)} \right) / \eta(0). \quad (18)$$

From (16) we conclude that the fixed point  $\eta = 0$  is stable. For libration around  $2n\pi$ ,  $n \neq 0$ , add  $2n\pi$  to (17). From (15) we have that

$$e_p(t) = e_p^{(eq)} [1 - A \sin(W_q t + \beta)] \equiv e_p^{(lib)}(t) \quad (19)$$

so that the maximum and minimum values of  $e_p$  when a system is librating are approximately

$$e_p^{max, min} = (1 \pm A) e_p^{(eq)}. \quad (20)$$

For libration about  $\eta = \pi$ , also a stable fixed point,

$$\eta(t) = \pi - A \cos(W_q t + \beta), \quad (21)$$

with  $A$  and  $\beta$ ,  $e_p(t)$  and  $e_p^{max, min}$  again given by (18), (19) and (20) respectively. For libration around  $(2n+1)\pi$ ,  $n \neq 0$ , add  $2n\pi$  to (21). Since  $W_q > 0$  for libration about  $\eta = 0$  and  $W_q < 0$  for libration about  $\eta = \pi$ , from (10) we have that

$$\frac{m_c}{m_p} > \sqrt{\frac{a_p}{a_c}} \varepsilon_c^{-1} \text{ for libration about } \eta = 0; \quad \frac{m_c}{m_p} < \sqrt{\frac{a_p}{a_c}} \varepsilon_c^{-1} \text{ for libration about } \eta = \pi. \quad (22)$$

Consider libration about  $\eta = 0$ . This can occur as long as there are solutions to  $\dot{\eta} = 0$ , that is, there exist real values for  $\eta$  when  $\cos \eta = (e_p/e_c) W_q / W_o$ . From (19) and (14) this is (in the linear approximation)

$$\cos \eta = 1 - A \sin(W_q t + \beta) \quad (23)$$

whose minimum value is  $1 - A$  (taking  $A$  to be positive) corresponding to the maximum value  $\eta$  achieves during a libration cycle. But in order for  $e_p$  to be positive or zero,  $0 \leq A \leq 1$  from (20). Thus we have the result that libration about  $\eta = 0$  can occur as long as  $|\eta| < \pi/2$ . Moreover, from (20) the maximum value of  $e_p$  associated with  $A = 1$ , and hence the value associated with the boundary between libration and circulation, is

$$e_p^{boundary} = 2 e_p^{(eq)} \quad (24)$$

which also holds for libration about  $\eta = \pi$ . In the latter case libration can occur as long as  $|\eta - \pi| < \pi/2$ . These results are consistent with numerically integrating the full equations (equations (4) to (7) but with the full dependence on  $e_p$ ; see Mardling (2007a)), an example of which is presented in Figure 1 for a system with  $m_p = 0.64 M_J$ ,  $m_c = 1 M_J$ ,  $m_* = 1.14 M_\odot$ ,

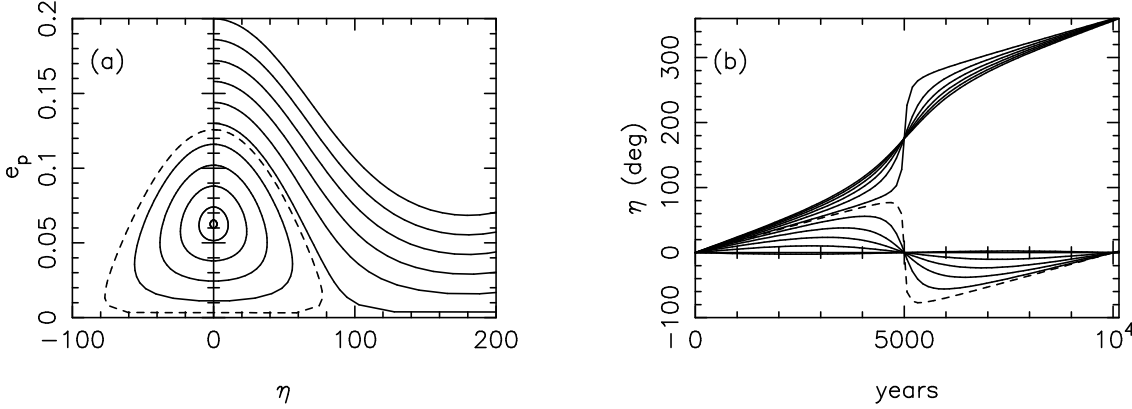


**Figure 1.** Evolution of  $e_p$  and  $\eta$  for an HD 209458 type system (parameters given in text). The full secular equations were integrated to produce these curves. (a) shows libration and circulatory behaviour consistent with  $e_p^{(eq)} = 0.063$  and  $e_p^{boundary} = 0.126$ , while (b) demonstrates that  $\dot{\eta}$  is almost constant for  $e_p(0)$  not too close to  $e_p^{boundary}$ . The dashed curve in both plots corresponds to  $e_p(0) = e_p^{boundary}$ . The libration and circulation periods are consistent with the analytical value of  $1.01 \times 10^4$  yr.

$a_p = 0.047$  AU,  $a_c = 0.4$  AU and  $e_c = 0.3$ . The values for the inner planet are appropriate for HD 209458b. Figure 1(a) plots  $e_p$  against  $\eta$  for  $\eta(0) = 0$  and 12 values of  $e_p(0)$  ranging from 0.06 to 0.2. Equation (14) gives  $e_p^{(eq)} = 0.063$  and  $e_p^{boundary} = 0.126$ . Figure 1(b) shows that for  $e_p > e_p^{boundary}$ ,  $\eta$  circulates with a frequency that is approximately constant ( $\simeq W_q$ ) as long as  $e_p$  is not too close to  $e_p^{boundary}$ . Putting  $\dot{\eta} = W_q$  gives

$$\eta(t) = W_q t + \eta(0), \quad (25)$$

so that from (8),  $\dot{e}_p = -W_o \sin(W_q t + \eta(0))$  and

$$e_p(t) = e_p(0) + (W_o/W_q) [\cos(W_q t + \eta(0)) - \cos \eta(0)] \equiv e_p^{(circ)}(t). \quad (26)$$

Therefore if  $W_q > 0$ , the maximum and minimum values of  $e_p$  correspond to  $\eta = 2n\pi$  and  $\eta = (2n+1)\pi$  respectively, where  $n$  is an integer, and are given by

$$e_p^{max,min} = e_p(0) \pm e_p^{(eq)} [1 \mp \cos \eta(0)], \quad (27)$$

while for  $W_q < 0$ , these are

$$e_p^{max,min} = e_p(0) \pm e_p^{(eq)} [1 \pm \cos \eta(0)] \quad (28)$$

corresponding to  $\eta = (2n+1)\pi$  and  $\eta = 2n\pi$  respectively. From (19) and (26) we see that both the libration and circulation periods are given by  $2\pi/W_q$ . For the example shown in Figure 1,  $2\pi/W_q = 1.01 \times 10^4$  yr.

The actual time variation of  $e_c$  can be obtained by forming  $de_p/de_c$  from (4) and (5), which upon integration gives

$$e_c(t) = \left[ 1 - (\beta e_p(t)^2 - C)^2 \right]^{1/2}, \quad (29)$$

where

$$\beta = \frac{1}{2} \sqrt{\frac{a_p}{a_c}} \left( \frac{m_p}{m_c} \right) \quad \text{and} \quad C = \beta e_p(0)^2 - \sqrt{1 - e_c(0)^2}, \quad (30)$$

and  $e_p(t)$  is given by (19) or (26) according to whether  $\eta$  librates or circulates.

Summarizing these results, we have that libration will occur about the fixed point  $(e_p, \eta) = (e_p^{(eq)}, 0)$  at frequency  $W_q > 0$  when

$$\frac{m_c}{m_p} > \sqrt{\frac{a_p}{a_c}} \varepsilon_c^{-1} \quad \text{and} \quad 0 \leq e_p < 2e_p^{(eq)} \quad \text{and} \quad -\pi/2 < \eta < \pi/2, \quad (31)$$

while libration will occur about the fixed point  $(e_p, \eta) = (e_p^{(eq)}, \pi)$  at frequency  $W_q < 0$  when

$$\frac{m_c}{m_p} < \sqrt{\frac{a_p}{a_c}} \varepsilon_c^{-1} \quad \text{and} \quad 0 \leq e_p < 2e_p^{(eq)} \quad \text{and} \quad \pi/2 < \eta < 3\pi/2. \quad (32)$$

Similar results hold for  $n \neq 0$ . If neither of the conditions (31) or (32) are met,  $\eta$  will circulate at frequency  $W_q$  with the maximum and minimum values of  $e_p$  given by (27) when  $m_c/m_p > \varepsilon_c^{-1} \sqrt{a_p/a_c}$  ( $W_q > 0$ ), and (28) when  $m_c/m_p < \varepsilon_c^{-1} \sqrt{a_p/a_c}$  ( $W_q < 0$ ).

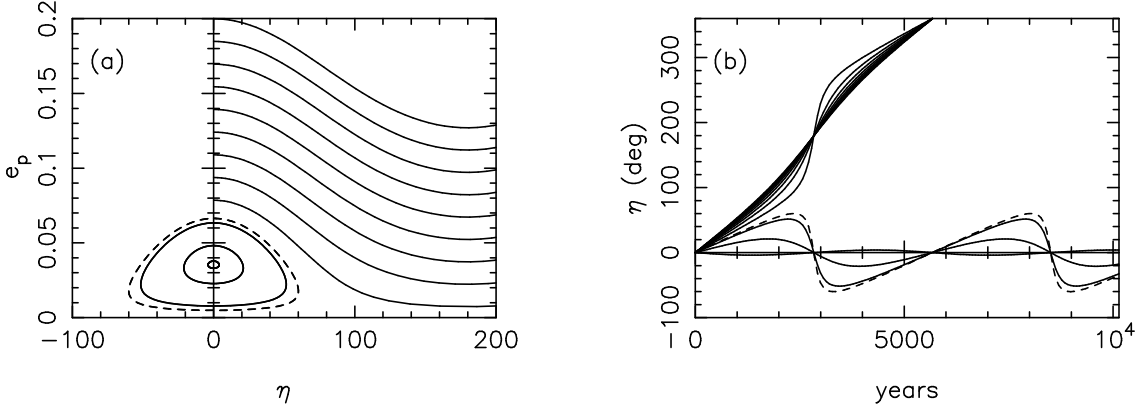


**Figure 2.** Same as Figure (1) but with  $W_{GR}$  included. Libration and circulation of  $\eta$  is more rapid and the maximum amplitude for librating systems is reduced in this case. The dashed curves correspond to  $e_p = e_p^{boundary}$ . The libration and circulation periods are consistent with the analytical value of 5700 yr.

### 3.2 Relativistic Effects

Contributions to the potential of the star from post-Newtonian terms affect the apsidal advance only. The orbit-averaged contribution to  $\dot{\eta}$  from the innermost orbit is (eg. Mardling & Lin, 2002)

$$W_{GR} = \frac{3n_p}{1 - e_p^2} \left( \frac{n_p a_p}{c} \right)^2, \quad (33)$$

where  $c$  is the speed of light, so that

$$\dot{\eta} = W_q + W_{GR} - W_o \left( \frac{e_c}{e_p} \right) \cos \eta \equiv \overline{W}_q - W_o \left( \frac{e_c}{e_p} \right) \cos \eta, \quad (34)$$

where

$$\overline{W}_q = \frac{3}{4} n_p \left( \frac{a_p}{a_c} \right)^3 \left( \frac{m_c}{m_*} \right) \varepsilon_c^{-3} \left[ 1 - \sqrt{\frac{a_p}{a_c}} \left( \frac{m_p}{m_c} \right) \varepsilon_c^{-1} + \gamma \varepsilon_c^3 \right], \quad (35)$$

and  $\gamma = 4(n_p a_p / c)^2 (m_* / m_c) (a_c / a_p)^3$  is, to first-order in  $e_p$ , the ratio of  $W_{GR}$  to the quadrupole contribution to  $\dot{\omega}_p$ . One effect of  $W_{GR}$  on the system is to shorten the eccentricity modulation and apsidal period (compare Figure 2 with Figure 1). In this example,  $W_{GR} \simeq W_q$  in contrast to Mercury's orbit around the Sun for which  $W_{GR}$  is only 7% of the contributions to  $\overline{W}_q$  from the other planets in the Solar System. The equilibrium eccentricity is now given by<sup>3</sup>

$$e_p^{(eq)} = e_c W_o / |\overline{W}_q| = \frac{(5/4)(a_p/a_c) e_c \varepsilon_c^{-2}}{\left| 1 - \sqrt{a_p/a_c} (m_p/m_c) \varepsilon_c^{-1} + \gamma \varepsilon_c^3 \right|}. \quad (36)$$

Thus when  $\sqrt{a_p/a_c} (m_p/m_c) \varepsilon_c^{-1} < 1$ , the effect of  $W_{GR}$  is to decrease the equilibrium eccentricity, an example of which is shown in Figure 2, while for  $\sqrt{a_p/a_c} (m_p/m_c) \varepsilon_c^{-1} > 1$  the opposite is true. Mardling & Lin (2004) show that the former can be vital for the survival of short period terrestrial planets with companions.

The analogues of (31) and (32) are that libration will occur about the fixed point  $(e_p, \eta) = (e_p^{(eq)}, 0)$  at frequency  $\overline{W}_q > 0$ , where  $e_p^{(eq)}$  is now given by (36), when

$$\frac{m_c}{m_p} > \sqrt{\frac{a_p}{a_c}} \varepsilon_c^{-1} / (1 + \gamma \varepsilon_c^3) \quad \text{and} \quad 0 \leq e_p < 2 e_p^{(eq)} \quad \text{and} \quad -\pi/2 < \eta < \pi/2, \quad (37)$$

while libration will occur about the fixed point  $(e_p, \eta) = (e_p^{(eq)}, \pi)$  at frequency  $\overline{W}_q < 0$  when

$$\frac{m_c}{m_p} < \sqrt{\frac{a_p}{a_c}} \varepsilon_c^{-1} / (1 + \gamma \varepsilon_c^3) \quad \text{and} \quad 0 \leq e_p < 2 e_p^{(eq)} \quad \text{and} \quad \pi/2 < \eta < 3\pi/2. \quad (38)$$

If neither of the conditions (37) or (38) are met, then when  $m_c/m_p > \varepsilon_c^{-1} \sqrt{a_p/a_c} / (1 + \gamma \varepsilon_c^3)$ ,  $\eta$  will circulate at frequency  $\overline{W}_q$  in the positive direction with the maximum and minimum values of  $e_p$  given by (27), while when  $m_c/m_p < \varepsilon_c^{-1} \sqrt{a_p/a_c} / (1 + \gamma \varepsilon_c^3)$ ,

<sup>3</sup> Note that equation (4) in Mardling & Lin (2004) is in error by a factor of 2.



$\eta$  will circulate in the negative direction at the same frequency with maximum and minimum values of  $e_p$  given by (28). The time variations of  $\eta$ ,  $e_p$  and  $e_c$  are given by the equations set out in the previous section, with  $e_p^{(eq)}$  given by (36).

The form of (36) suggests that for a range of parameters,  $e_p^{(eq)}$  can be large. Singular values of  $e_p^{(eq)}$  exist for some combinations of parameters, although when the octopole term in (7) is included in (9) these are replaced by finite, although still relatively large values (see Nagasawa, Lin & Ida (2003)). As we will show in Section 3.3.4, this has important consequences for eccentricity forcing by low-mass companions.

### 3.3 Tidal damping and quasi-fixed-point behaviour

While tidal dissipation in the innermost planet directly affects the rate of change of its eccentricity, it also indirectly affects the rate of change of the companion planet's eccentricity (recall that the previous analysis assumed  $e_c$  was constant), as well as the angle between the apsidal lines,  $\eta$ .<sup>4</sup> The relevant system of equations now becomes

$$\dot{e}_p = -W_o e_c \sin \eta - W_T e_p, \quad (39)$$

$$\dot{e}_c = W_c e_p \sin \eta, \quad (40)$$

$$\dot{\eta} = \overline{W}_q - W_o \left( \frac{e_c}{e_p} \right) \cos \eta, \quad (41)$$

where from (2),

$$W_T = \frac{21}{2} n_p \left( \frac{k_p}{Q_p} \right) \left( \frac{m_*}{m_p} \right) \left( \frac{R_p}{a_p} \right)^5 = \tau_{circ}^{-1} \quad (42)$$

and from (7),

$$W_c = \frac{15}{16} n_c \left( \frac{m_p}{m_*} \right) \left( \frac{a_p}{a_c} \right)^3 \varepsilon_c^{-4}, \quad (43)$$

where again we have ignored the octopole term (proportional to  $e_p/e_c$ ) in (7). The damped autonomous system (39)-(41) evolves to the formal fixed point  $(e_p, e_c, \eta) = (0, 0, \eta^*)$ , where  $\eta^*$  is given below and is such that  $|\eta^*|(\bmod 2\pi) \ll 0$  or  $|\eta^* - \pi|(\bmod 2\pi) \ll 0$  for  $\overline{W}_q > 0$  and  $\overline{W}_q < 0$  respectively. However, there are three timescales associated with this evolution: (1) The system circulates until  $e_p$ ,  $e_c$  and  $\eta$  are such that libration conditions are met (see (31) and (32): the system is “captured” by the associated fixed point). This occurs on the circularization timescale of the inner orbit,<sup>5</sup>  $\tau_{circ}$ ; (2) The system librates about and evolves towards the (now quasi-)fixed point  $(e_p, e_c, \eta) = (e_p^*, e_c^*, \eta^*)$ , where  $e_c^* \simeq e_c(0)$  and  $e_p^* \simeq e_p^{(eq)}$  (equation (36)), on the timescale  $2\tau_{circ}$  ( $e_c^*$  and  $e_p^*$  will be properly defined below); (3) The system evolves smoothly towards the formal fixed point  $(e_p, e_c, \eta) = (0, 0, \eta^*)$  on some timescale  $\tau_c \gg \tau_{circ}$ . The details for these phases are as follows, where for the first two we assume that  $\dot{e}_c \ll \dot{e}_p$  so that  $e_c \simeq e_c(0)$ .

#### 3.3.1 Circulation

Following Section 3.1.1, the circulation phase can be approximated with  $\dot{\eta} = \overline{W}_q$ . Then (39) becomes

$$\dot{e}_p + W_T e_p = -W_o e_c \sin(\overline{W}_q t + \eta(0)) \quad (44)$$

which has solution

$$e_p(t) = C e^{-W_T t} + \sigma e_p^{(eq)} \cos(\overline{W}_q t + \eta(0)) \quad (45)$$

where  $\sigma = \text{sgn}[\overline{W}_q]$ ,  $C = e_p(0) - \sigma e_p^{(eq)} \cos \eta(0)$  and we have assumed that  $W_T \ll |\overline{W}_q|$ . This phase is shown in blue in Figure 3 and evolves on the timescale  $1/W_T = \tau_{circ}$ . Notice that the amplitude of variation is not affected by dissipation and is given by  $e_p^{(eq)}$ . Also note that  $Q_p$  is set artificially low in order to clearly demonstrate how this phase proceeds.

#### 3.3.2 Libration

The quasi-fixed point  $(e_p^*, e_c^*, \eta^*)$  is obtained by putting  $\dot{e}_p = 0$  and  $\dot{\eta} = 0$  in (39) and (41) respectively. While there is only one true equilibrium value of  $e_c$  (that is,  $e_c = 0$ ), we take  $e_c^*$  to be the value of  $e_c$  when the libration amplitude of  $e_p$  drops below some specified small value (see next section). Eliminating  $e_p/e_c$  between (39) and (41) then gives

<sup>4</sup> The contributions to  $\dot{\eta}$  from the tidal and spin bulges of the star and planets are negligible compared to the terms included here.

<sup>5</sup> This phase is skipped if the initial conditions are such that the system starts librating immediately.

$$\sin \eta^* = -\frac{W_T}{\overline{W}_q} \cos \eta^* \simeq -\frac{W_T}{|\overline{W}_q|} < 0, \quad (46)$$

where the second step comes from the fact that  $\text{sgn}(\cos \eta^*) = \text{sgn}(\overline{W}_q)$  and  $W_T/|\overline{W}_q| \ll 1$ . Thus for  $\overline{W}_q > 0$ ,  $\eta^* \pmod{2\pi} \simeq -W_T/\overline{W}_q$  while for  $\overline{W}_q < 0$ ,  $(\eta^* - \pi) \pmod{2\pi} \simeq -W_T/\overline{W}_q$ . For HD 209458b with a  $0.1M_J$  companion at 0.4 AU,  $\eta^* = 10^{-5} - 10^{-4}$ , depending on the value of  $e_c$  (taking  $Q_p = 10^5$ ). The value of  $e_p^*$  is given by (36) with  $e_c = e_c^*$ . Linearizing about  $(e_p^*, e_c^*, \eta^*)$  and putting  $x = e_p - e_p^*$  and  $y = \eta - \eta^*$  produces the system

$$\dot{x} = -e_c^* W_o y - W_T x, \quad (47)$$

$$\dot{y} = (\overline{W}_q^2 / e_c^* W_o) x, \quad (48)$$

which yields the damped librating solution

$$e_p(t) = e_p^* + A e^{-W_T t/2} \cos(W_q t + \delta) \quad (49)$$

and

$$\eta(t) = \eta^* - A e^{-W_T t/2} \sin(W_q t + \delta). \quad (50)$$

For the purposes of this analysis, the constants  $A$  and  $\delta$  can be taken to be such that the librating phase is entered at the first occurrence of  $e_p = 0$ . Writing the time at which this occurs as  $t = t_{lib}$ , (49) and (50) become

$$e_p(t) = e_p^* \left\{ 1 - e^{-W_T(t-t_{lib})/2} \cos[W_q(t-t_{lib})] \right\} \quad (51)$$

and

$$\eta(t) = \eta^* - e^{-W_T(t-t_{lib})/2} \sin[W_q(t-t_{lib})] \quad (52)$$

In contrast to the circulating phase, the amplitude of oscillation of  $e_p(t)$  diminishes on a timescale  $2/W_T = 2\tau_{circ}$  as the system approaches the quasi-fixed point. Figure 3 shows this behaviour in red.

For the analysis above we have assumed  $e_c$  is constant. However, as Figure 3(c) illustrates,  $e_c$  slowly declines and has no analogue of  $e_p^{(eq)}$  (except  $e_c = 0$ ). The following section studies the effect of this on the long-term evolution of the system.

### 3.3.3 Long-term evolution

Once the quasi-fixed point is reached, the companion's eccentricity evolves according to (40) with  $e_p = e_c W_o / |\overline{W}_q|$  and  $\sin \eta = -W_T / |\overline{W}_q|$ :

$$\begin{aligned} \dot{e}_c &= -\frac{W_c W_o W_T}{\overline{W}_q^2} e_c \\ &= -\left(\frac{25}{16}\right) \left(\frac{m_p}{m_c}\right) \left(\frac{a_p}{a_c}\right)^{5/2} W_T \cdot \frac{e_c}{F(e_c)} \\ &= -\left(\frac{\lambda}{\tau_{circ}}\right) \frac{e_c}{F(e_c)} \end{aligned} \quad (53)$$

where

$$\lambda = \left(\frac{25}{16}\right) \left(\frac{m_p}{m_c}\right) \left(\frac{a_p}{a_c}\right)^{5/2} \quad \text{and} \quad F(e_c) = \varepsilon_c^3 (1 - \alpha \varepsilon_c^{-1} + \gamma \varepsilon_c^3) \quad (54)$$

with  $\alpha = \sqrt{a_p/a_c} (m_p/m_c)$  (recall that  $\varepsilon_c = \sqrt{1 - e_c^2}$ ). Note that  $\alpha$  and  $\gamma$  are effectively constant throughout the evolution since the semimajor axes evolve on timescales much longer than the age of the system (see Figure 5(d)). One can obtain an approximate timescale on which  $e_c$  (and hence  $e_p$ ) evolves by putting  $\varepsilon_c \simeq \varepsilon(e_c^*) \equiv \varepsilon_c^*$ , where  $e_c^*$  is yet to be formally defined. Equation (53) then gives

$$e_c(t) = e_c(t_c) e^{-(t-t_c)/\tau_c}, \quad (55)$$

where

$$\tau_c = (F(e_c^*)/\lambda) \tau_{circ} \quad (56)$$

and  $t_c$  corresponds to the beginning of the slow evolution phase which we choose to be the first instance of  $|\eta - \eta^*| < \epsilon$  for all  $t > t_c$ . Here  $\epsilon \ll 1$  is an arbitrarily chosen parameter and is taken to be  $\epsilon = 10^{-4}$  for the studies presented in this paper. This then serves as definitions of  $e_c^*$  and  $e_p^*$ , that is,  $e_c^* = e_c(t_c)$  and  $e_p^* = e_p(t_c)$ . The transition to the slow phase at time  $t_c$  is indicated in Figures 3(b)-(d) by a diamond symbol. Note that  $\tau_c \gg \tau_{circ}$  for most stable systems, except when  $F(e_c)$  is small (see Section 3.3.4). The approximate solution (55) is the blue dot-dashed curve in Figure 4(a).

Keeping the full dependence on  $e_c$  in (53) and integrating gives

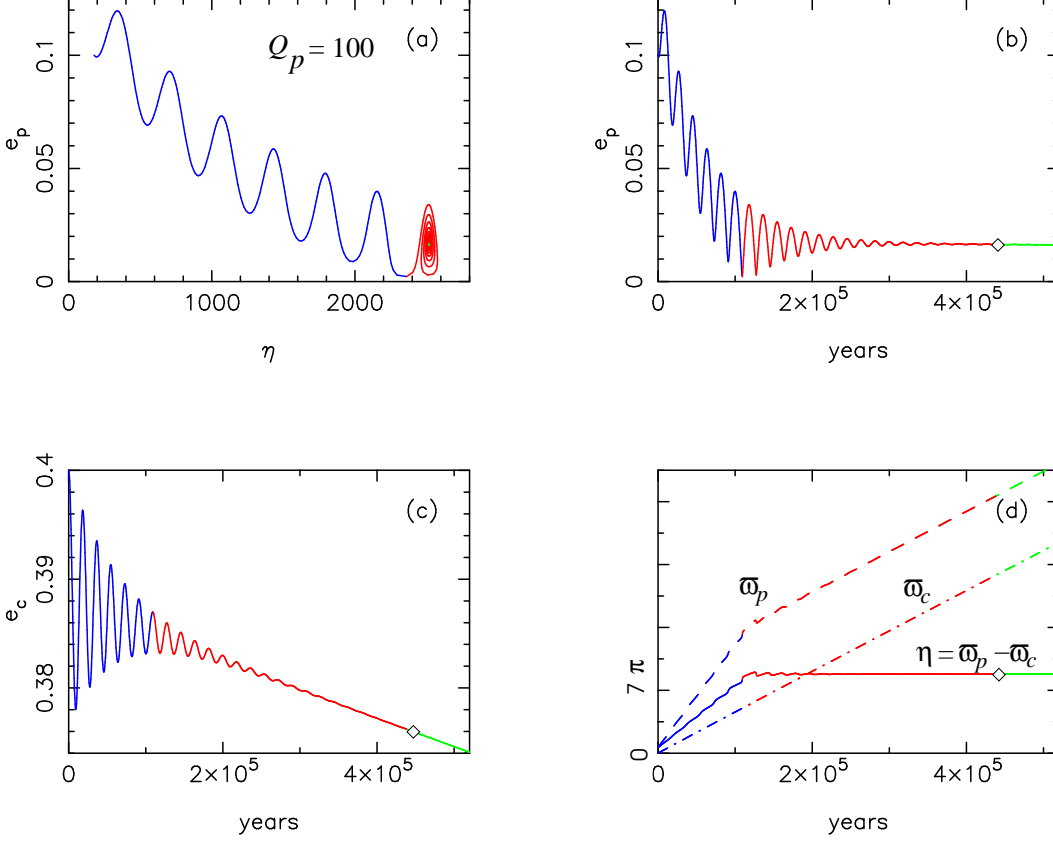


**Figure 3.** Capture phase for HD 209458b with a  $0.1M_J$  companion at 0.4 AU with  $e_c = 0.4$ . The full secular equations including evolution of  $a_p$  and  $a_c$  are integrated (Mardling & Lin 2004). The  $Q$ -value of the observed planet is set artificially low at  $Q_p = 100$  in order to illustrate the process (timescales are linearly proportional to  $Q_p$  and values for  $e_c^*$  are not very sensitive to the value of  $Q_p$ ; for this example, the relative change in  $e_c^*$  is less than 2% over four orders of magnitude in  $Q_p$ ). Blue curves correspond to the circulation phase, red to the libration phase and green to the slow evolution or quasi-fixed point phase (see text for more discussion). In panel (c) notice that the relative change in  $e_c$  is small, justifying (at least for this example) taking  $e_c \simeq \text{const}$  during this phase in the analysis. The diamond symbols correspond to the points  $(t_c, e_p^*)$ ,  $(t_c, e_c^*)$  and  $(t_c, \eta^*)$  in panels (b), (c) and (d) respectively. Panel (d) shows the apsidal advance of the inner and outer orbits, with  $\tilde{\omega}_p$  locking onto  $\tilde{\omega}_c$ . This occurs irrespective of the mass of the outer body because  $e_p/e_c \ll 1$  (see equation (7)).

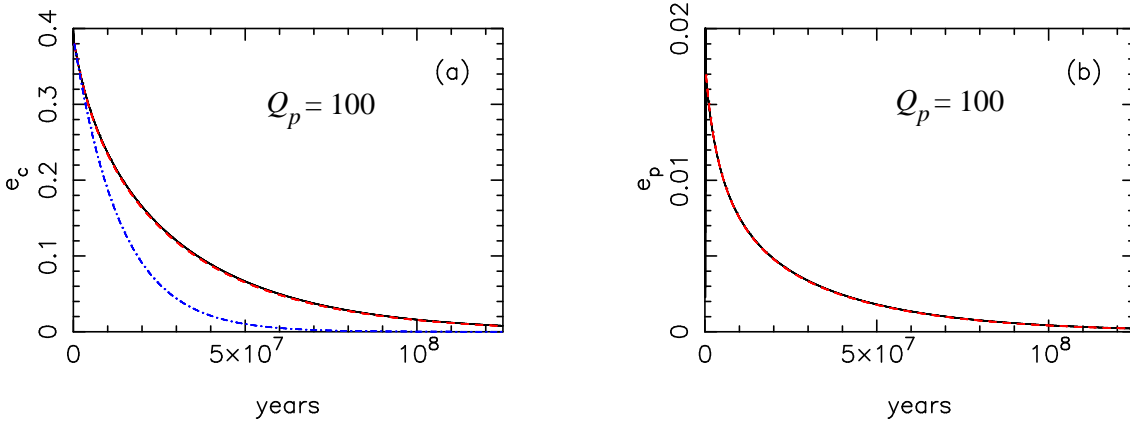


**Figure 4.** Continuation of numerical solution in Figure 3 showing the long-term evolution of (a)  $e_c$  and (b)  $e_p$  (black curves, sitting underneath red curves), again with  $Q_p = 100$  for illustration (note the  $y$ -axis scales are different to those in Figure 3). This corresponds to 125 Gyr of evolution when  $Q_p = 10^5$  (compare this to  $\tau_{\text{circ}} = 0.045$  Gyr). Also plotted in (a) is approximate solution (55) (blue dot-dash curve) and the analytic solution (58) (dashed red curve). The approximate solution underestimates the timescale on which  $e_c$  evolves by a factor of 1.8. Also plotted in (b) is the analytic expression for  $e_p(t)$  (red curve) using (36) with  $e_c = e_c(t)$  from (58). The analytic solutions are essentially indistinguishable from the numerical solutions.

$$f(e_c; \alpha, \gamma) - f(e_c^*; \alpha, \gamma) = -\lambda(t - t_c)/\tau_{circ}, \quad (57)$$

where

$$\begin{aligned} f(x; \alpha, \gamma) = & -\frac{1}{3}\gamma x^6 + \frac{3}{2}\gamma x^4 + (\alpha - 3\gamma)x^2 + \sqrt{1-x^2} \left[ \alpha^2 - \frac{42}{315}\gamma(3x^4 - 11x^2 + 23)\alpha - \frac{1}{3}(x^2 - 4) + \gamma^2 g(x) \right] \\ & + (\gamma - \alpha + 1)^2 \ln x - [(\gamma - \alpha)^2 + 1] \ln \left( 1 + \sqrt{1-x^2} \right) \end{aligned} \quad (58)$$

with

$$g(x) = (35x^8 - 185x^6 + 408x^4 - 506x^2 + 563)/315. \quad (59)$$

This solution is shown as a dashed red curve in Figure 4(a) and is clearly superior to the estimate (55) which *underestimates* the timescale on which the system evolves once apsidal locking has taken place. We define the true timescale on which circularization of the companion orbit takes place (the  $e$ -folding time) to be the time corresponding to  $e_c^*/e$ , that is, from (57),

$$\tau_c^{true} = \left[ 3 + \lambda^{-1} (f(e_c^*; \alpha, \gamma) - f(e_c^*/e; \alpha, \gamma)) \right] \tau_{circ}, \quad (60)$$

where we have put  $t_c = 3\tau_{circ}$  (1 for the circulation phase + 2 for the libration phase). As  $e_c$  slowly decreases,  $e_p$  maintains a value given by (36). Any departure from this quasi-equilibrium value is quickly damped out on the circularization timescale  $\tau_{circ}$ . Thus we can use (57) and (36) to calculate analytically  $e_c(t)$  and  $e_p(t)$  during the slow phase, and hence to determine the current value of  $e_p$  using the estimated age of the system. The analytic solution for  $e_p(t)$  is shown in Figure 4(b) (red curve) and is indistinguishable from the numerical solution.

### 3.3.4 The increasing $e_p$ regime: very low-mass companions

The solution for the example given in Figure 4 is essentially a modified decaying exponential. However, there is another regime of the function  $f(x; \alpha, \gamma)$  which behaves very differently and is associated with very low-mass companions which, for a large part of the life of such systems, force  $e_p$  to *increase* to some maximum value before decaying to zero at the end of the tidally evolving phase. An example of this is shown in Figure 5 for the HD 209458 system with a companion of mass  $m_c = 0.0125M_J = 4.2M_\oplus$  at  $a_c = 0.3$  AU and an *initial* companion eccentricity of 0.7, a high value chosen to clearly illustrate the theory. The system enters the slow phase with  $e_c^* = 0.705$ ,  $e_p^* = 0.013$  and  $\eta^* \simeq -43\pi$ . The average reflex velocity of the star due to the companion is  $0.64 \text{ m s}^{-1}$ . See the figure caption for a detailed description of the evolution of the system. The red dashed curves again represent the analytic solutions (58) and (36), clearly demonstrating their predictive power. In fact, the analytic solution for  $e_p$  passes through a singularity as the denominator in (36) passes through zero. The full numerical solution avoids this, but still manages to increase to a significant level on a reasonably long timescale. For  $Q_p = 10^5$ , passage through the “singularity” occurs at 2.2 Gyr, well before the system age of 5.5 Gyr, while for  $Q_p = 2 \times 10^5$ , passage through this point occurs “now”. Note that this system is stable when the full three-body (non-secular) equations are integrated including post-Newtonian relativistic terms, tidal and spin bulges, as well as tidal damping (Mardling & Lin 2002).

Although systems which pass through the singularity suffer a rapid decline in  $e_p$  once they have done so, they tend to maintain the value of  $e_p^*$  at the beginning of the slow phase before this happens (see also Figure 6). This is in contrast to systems which don’t pass through the singularity; these simply decay approximately exponentially. To determine the parts of parameter space for which  $e_p$  necessarily passes through the singularity and therefore maintains  $e_p^*$  before it does so, and in particular which systems pass through the singularity *after* the current age of the system, we start by studying the behaviour of the denominator of (36). Defining

$$\Delta(e_c; \alpha, \gamma) = 1 - \alpha e_c^{-1} + \gamma e_c^3, \quad (61)$$

where (again),  $\alpha = \sqrt{a_p/a_c}(m_p/m_c)$ , Figure 7 plots this function against  $m_c$  for specific values of  $a_c$  and for  $e_c = 0.8$  and  $e_c = 0$ . There are three regimes of interest. As the system evolves from  $e_c^*$  down to  $e_c = 0$ , either (a)  $\Delta$  (and hence  $\overline{W}_q$ ) remains negative so that  $\cos \eta \simeq -1$  always (blue arrow); (b)  $\Delta$  passes through zero so that  $\eta$  goes through a short period of circulation as  $\cos \eta$  passes from -1 to 1 (yellow background, red arrows) or (c)  $\Delta$  is positive always and  $\cos \eta \simeq 1$  (green arrows). In the case shown here ( $e_c^* = 0.8$ ), systems cross  $\Delta = 0$  for a finite range of values of  $m_c$  when  $a_c \lesssim 0.29$ ; when  $0.29 \lesssim a_c \lesssim 0.52$ , all systems with  $m_c$  less than some critical value cross  $\Delta = 0$ ; when  $a_c \gtrsim 0.52$  no systems cross  $\Delta = 0$ . Figure 7(b), for example, shows that all systems with  $m_c \lesssim 0.25M_J$  and  $a_c = 0.3$  (and  $e_c^* = 0.8$ ) necessarily evolve through  $\Delta = 0$ . The ranges above vary with different values of  $e_c^*$ ; curves corresponding to  $e_c^* < 0.8$  lie between the two shown. What remains to be determined, however, is which of these systems maintain a non-zero value of  $e_p$  for at least as long as the current age of the system before they do so. Once this is done, the parameter ranges should be further restricted by determining which systems are stable (Mardling 2007b).

Figure 8 plots  $e_p(\text{now})$ ,  $e_p(t_c)$  and  $e_c(\text{now})$  against companion mass for the HD 209458 system for various values of  $a_c$  and  $e_c^*$ . Here “now” refers to  $t = 5.5$  Gyr, and the quantities are calculated using (36) and (58). The green-filled circle corresponds

HD 209458:  $a_c = 0.3$ ,  $e_c = 0.7$ ,  $m_c = 4.2 M_\oplus$ ,  $Q_p = 100$

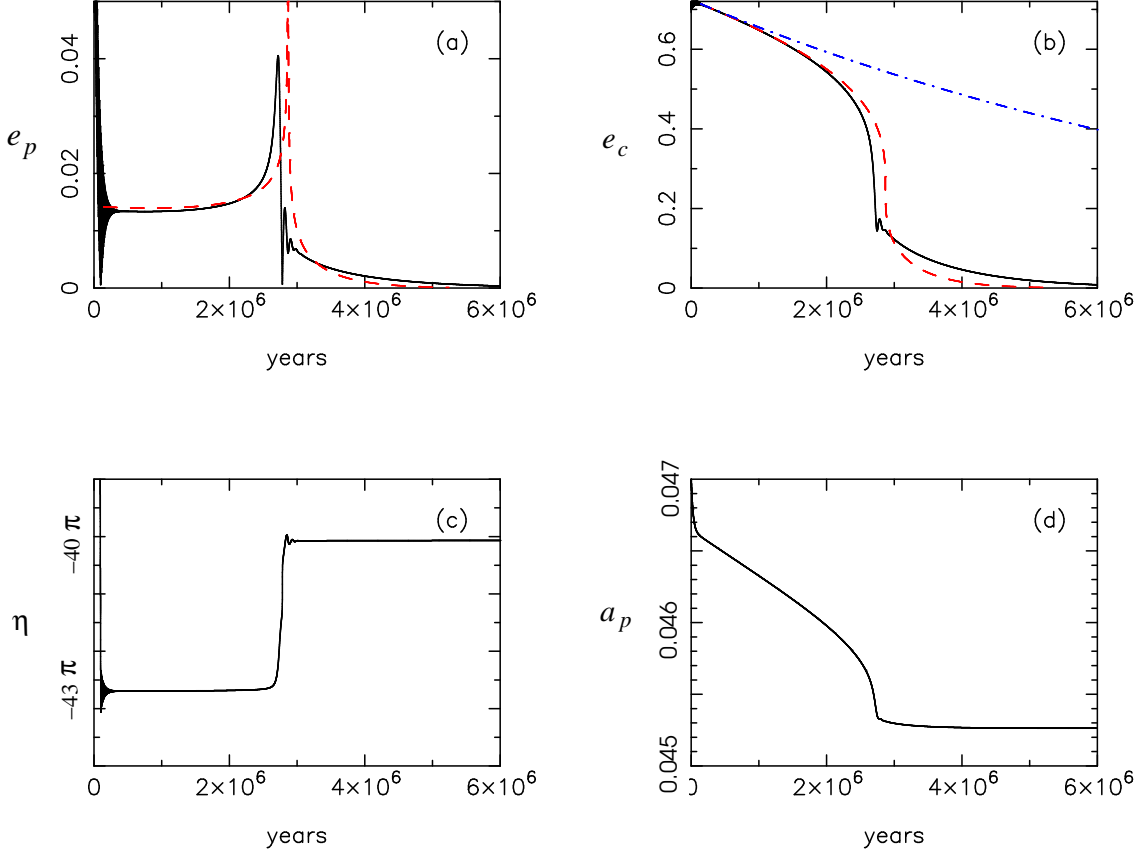
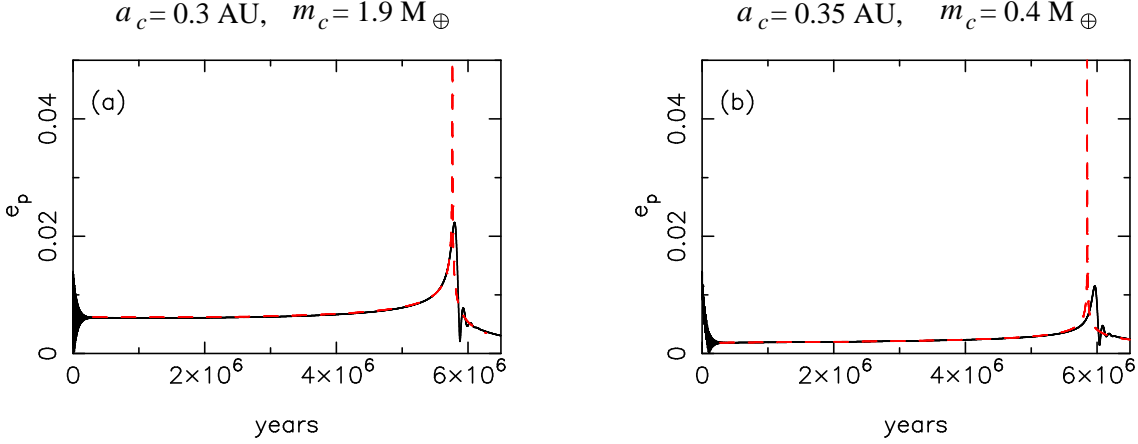


**Figure 5.** A terrestrial-mass planet can sustain the observed eccentricity of HD 209458 - but not for long enough in this example where  $m_c = 4.2 M_\oplus$ , at least for  $Q_p \lesssim 2 \times 10^5$ . The black curves show the numerical solutions while the red dashed curves are given by the analytical solutions (36) for  $e_p$  and (58) for  $e_c$ . (a): The evolution of  $e_p$  following capture. After effectively maintaining the value  $e_p^* \simeq 0.013$  for some 2 Gyr (for  $Q_p = 10^5$ ),  $e_p$  increases to a maximum of around 0.04 before rapidly declining to around 0.008 and then slowly declining to zero. The increase in  $e_p$  corresponds to a singularity in the analytic solution which fairly accurately follows the full solution. Recall that the actual timescale is proportional to  $Q_p$ . The fact that the analytical solution is reliable confirms this dependence. Thus, for  $Q_p = 10^5$ , the maximum value of  $e_p$  occurs around 2.7 Gyr. Recall also that the value of  $e_p$  at the beginning of the slow phase is quite insensitive to  $e_p(0)$ ,  $\eta(0)$  and  $Q_p$ . (b): The evolution of  $e_c$  following capture. Again the analytic solution is a good approximation to the full solution. The blue dot-dashed curve is the approximate analytic solution given by (55). Thus when a system must pass through the singularity, the timescale given by (56) overestimates the circularization timescale in contrast to the previous example. (c): The evolution of  $\eta = \varpi_p - \varpi_c$ . During the pre-capture phase,  $\eta$  circulates backwards before being captured at  $\eta = -43\pi$  (recall that when  $\bar{W}_q < 0$ ,  $\cos \eta \simeq -1$ ). As the system passes through the singularity, that is, as  $\bar{W}_q$  passes through zero to become positive (see equation (35)),  $\eta$  circulates back up to  $-40\pi$  so that  $\cos \eta \simeq 1$ . The brief circulatory period is accompanied by oscillations in  $e_p$  and  $e_c$  which can be seen in (a) and (b). (d): The evolution of  $a_p$ . The full (secular) numerical solution includes the evolution of both semimajor axes; here we see that over the entire evolution of this system,  $a_p$  changes by less than 4%.

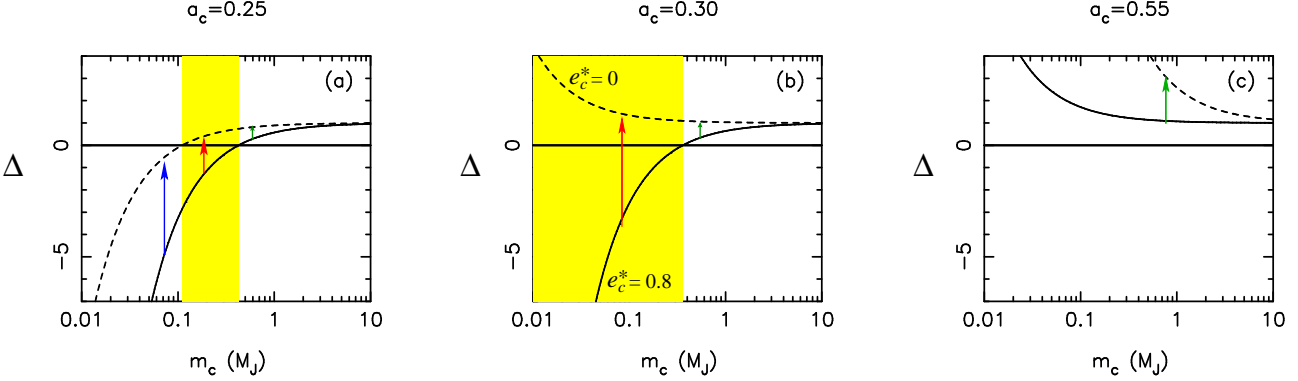
to the system shown in Figure 5 at  $t = 5.5$  Gyr for  $Q_p = 10^5$  ( $t = 5.5$  Myr for  $Q_p = 10^2$ ), while the red-filled circles correspond to Figure 6 at the same time. Note the extremely low companion masses in Figures 6(a) and (b):  $m_c = 1.9 M_\oplus$  and  $m_c = 0.4 M_\oplus$  respectively. The maximum values of  $e_p$  achieved are (a) 0.022 at 5.8 Gyr and (b) 0.012 at 6.0 Gyr. The corresponding values of  $e_c$  are 0.27 and 0.50. At 5.5 Gyr, the values for  $e_p$  are (a) 0.010 and (b) 0.004, with corresponding values for  $e_c$  of 0.41 and 0.60. Thus scenario (a) represents a possible solution for HD 209458 for a value of  $Q_p$  around  $10^5$ , while scenario (b) requires a  $Q$ -value around 10% smaller in order that the maximum value of  $e_p$  occurs about now (recall that this also depends on the age estimate for the star). Figure 8 demonstrates that high initial values of  $e_c^*$  are required in order that extremely low-mass companions be responsible for maintaining the eccentricity of inflated planets (see Section 6 for a discussion on this point).

Figure 8, together with Figures 5 and 6 and equation (60), suggest that for given values of  $a_c$  and  $e_c^*$ , the time a system takes to achieve its maximum value of  $e_p$  (given it passes through  $\Delta = 0$ ) increases as the companion mass decreases. Figure 9 plots this time,  $T_{\text{evol}}$ , as a function of  $m_c$  for various values of  $a_c$  and  $e_c^*$  (solid curves). Also plotted is  $\tau_c^{\text{true}}$  (equation (60))

$$\text{HD 209458: } e_c(0) = 0.7, \quad Q_p = 100$$



**Figure 6.** Similar to Figure 5 but with lower values for  $m_c$ . Passage through  $\Delta = 0$  occurs later in the life of the system (compare panel (a) to Figure 5(a)), while  $e_p^*$  is smaller. For (a), the maximum value of  $e_p = 0.022$  is reached at 5.8 Gyr for  $Q_p = 10^5$ , while at 5.5 Gyr,  $e_p = 0.010$ . For (b),  $e_p = 0.012$  at 5.96 Gyr, while  $e_p = 0.004$  at 5.5 Gyr.



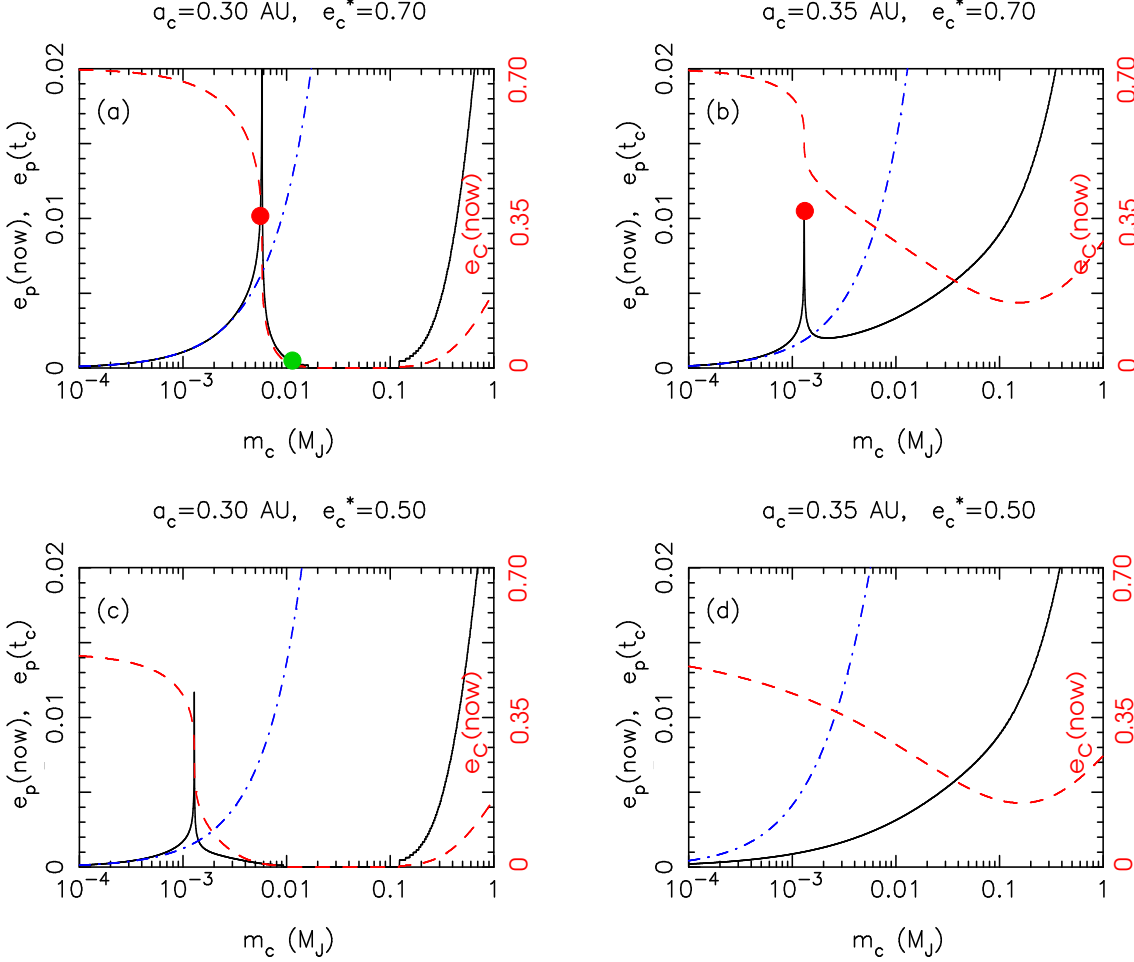
**Figure 7.** Behaviour of the denominator of (36),  $\Delta$ , used to determine which configurations have  $e_p^{(eq)}$  necessarily passing through a “singularity” during their evolution. See text for discussion. Note that some of the systems represented here are not stable when the full three-body equations are integrated with appropriate damping (Mardling & Lin 2002).

which is the  $e$ -folding time for systems which don’t go through  $\Delta = 0$  but simply decay approximately exponentially (dashed curves). The small values of  $T_{\text{evol}}$  corresponding to, for example, systems for which  $e_c^* = 0.5$  and  $a_c = 0.34$  with  $m_c \lesssim 0.002M_J$  (the dark blue curve which appears coincident with the  $x$ -axis), compared with the large values of  $T_{\text{evol}}$  for  $m_c \gtrsim 0.003M_J$ , simply indicate that passage through  $\Delta = 0$  occurs early in the life of the system, while decay following passage is very slow. Figure 10 illustrates this with the above example. The blue diamond indicates the nominal beginning of the slow phase (as defined in the discussion following equation (56)). There is little difference between Figures 10(a) and (b) except that 10(b) does not meet the slow phase criterion until after the system passes through  $\Delta = 0$ .

#### 4 CONSTRAINTS ON ORBITAL PARAMETERS OF COMPANIONS

We are now in the position to constrain the orbital parameters and masses of possible companion planets to HD 209458b, HAT-P1b and WASP-1b. Given estimated ages, our aim is to find initial conditions and companion masses for which these planets have eccentricities in the ranges observed (WASP-1b is currently unconstrained), and in the case of HD 209458, produces a stellar reflex velocity less than  $10 \text{ m s}^{-1}$  (an upper limit which gives companion masses less than the upper bound of  $0.3M_J$  cited in Laughlin et al. (2005a)).

Acknowledging again that these systems are unlikely to be exactly coplanar (but see Figure 16 which shows that moderate inclination has little effect), we assume zero mutual inclination and vary the parameters  $a_c$ ,  $m_c$  and  $e_c(0)$ . Our results correspond to the case  $e_p(0) = 0.1$  and  $\eta = 170^\circ$ , but are not very sensitive to using other values of these parameters (ie, they

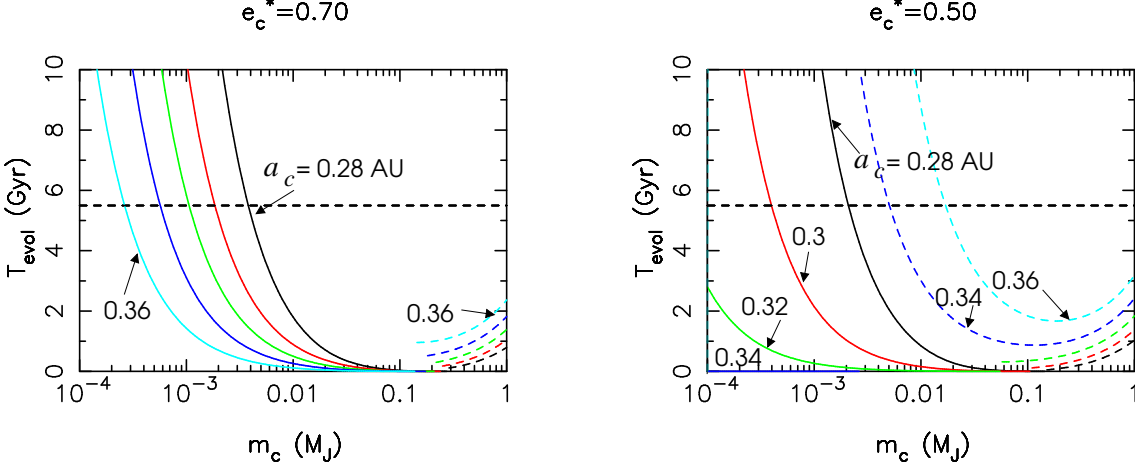
HD 209458: age = 5.5 Gyr,  $Q_p = 10^5$ 

**Figure 8.** The values of  $e_p$  and  $e_c$  (black solid and red-dash curves respectively) at  $t = 5.5$  Gyr, and the value of  $e_p$  at the beginning of the slow phase ( $e_p(t_c)$ : blue dot-dash curves), all with  $Q_p = 10^5$ . From Figures 5 and 6 it is evident that systems which pass through  $\Delta = 0$  in their lifetime approximately maintain their value of  $e_p$  at  $t = t_c$  before they do so. Thus, for example, in (a) all systems with  $m_c \lesssim 0.004 M_J$  will have the same finite (but small) eccentricities they had when they entered the slow phase. For a small range of masses ( $0.004 < m_c/M_J < 0.006$ )  $e_p(\text{now}) > e_p^*$  (the black curve sits above the blue curve), while for greater masses  $e_p(\text{now}) \ll e_p^*$ . Note that formally these curves have no upper bound at the point corresponding to  $\Delta = 0$ , however the finite resolution of the plots suggest erroneously that they do. In reality there does exist an upper bound when the secular equations are directly integrated as is evident in Figures 5 and 6. It is clear from this figure that high initial values of  $e_c^*$  are required to have very low-mass companions responsible for maintaining the eccentricity of inflated planets, although lower values of  $e_c^*$  are required for lower values of  $a_c$  (see Figure 13 and Section 6 for a discussion on this point).

evolve to the quasi-fixed point  $(e_p^*, e_c^*, \eta^*)$  initially with a variation in  $e_c^*$  of at most around 10%). Note also that while our aim is to determine whether or not current-day solutions exist (especially for HD 209458 which is the most constrained), we can also say something about the orbital elements at earlier times and hence (cautiously) constrain the initial conditions.

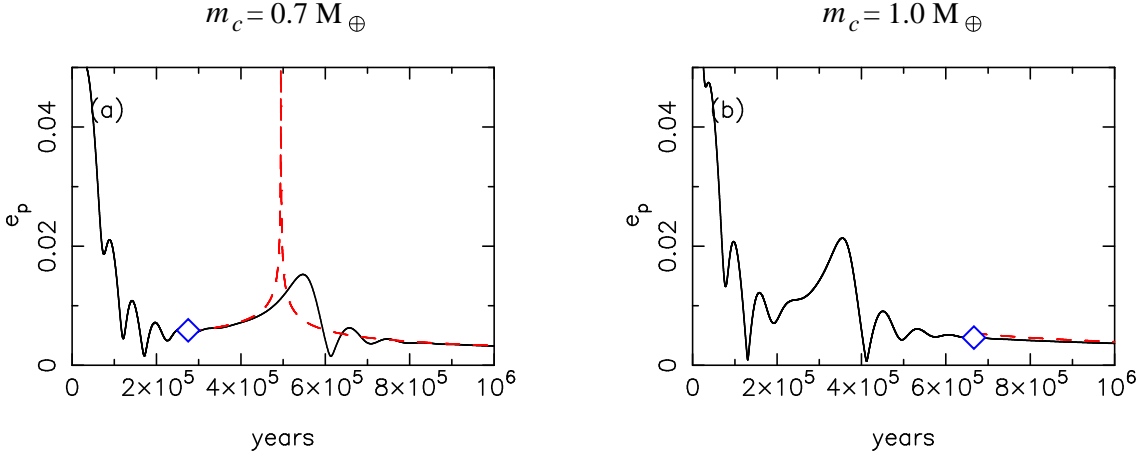
#### 4.1 HD 209458

Figure 11 presents results for  $\eta(0) = 170^\circ$ ,  $e_p(0) = 0.1$ ,  $0.3 \leq e_c(0) \leq 0.8$ ,  $0.02 \leq m_c/M_J \leq 0.2$  and  $0.1 \leq a_c/\text{AU} \leq 0.8$ . The full secular equations (Mardling 2007a) were integrated with  $Q_p = 100$  until  $e_c^*$  was reached and the value for this was used in (58) to calculate the current value of  $e_c$  (“ $e_c(\text{now})$ ”) and hence of  $e_p$  (“ $e_p(\text{now})$ ”) via (36) for a given *actual*  $Q$ -value ( $Q_p = 10^5$ ). Recall from the discussion in Section 3.3 that timescales scale linearly with  $Q_p$  and that *the relative change in  $e_c^*$  is less than 2% over four orders of magnitude in  $Q_p$* . Each point in the  $m_c - a_c$  plane is coloured according to  $e_p(\text{now})$  (top six panels) and  $e_c(\text{now})$  (bottom six panels). Also shown are boundaries for stellar reflex velocities *at periastron*  $v_*^p = 10 \text{ m s}^{-1}$  and  $v_*^p = 5 \text{ m s}^{-1}$ . Defining a “solution” to be a configuration for which  $e_p(\text{now}) > 0.010$ , solutions exist below  $v_*^p = 10 \text{ m s}^{-1}$



**Figure 9.** The time to reach the maximum value of  $e_p$ ,  $T_{evol}$ , for systems which pass through  $\Delta = 0$  (solid curves), and the evolution timescale (defined as the time corresponding to  $e_c = e_c^*/e$ ) for systems which do not (dashed curves). Various values of  $a_c$  are indicated on the plots; the estimated age of HD 209458 is indicated by the horizontal dashed line. The lower the companion mass, the longer the system takes before it passes through  $\Delta = 0$  (given that it does so at all). This phenomenon favours systems with high values of  $e_c^*$ .

HD 209458:  $a_c = 0.34$  AU,  $e_c(0) = 0.5$ ,  $Q_p = 100$



**Figure 10.** Demonstration that for some systems, passage through  $\Delta = 0$  occurs very early on in the evolution, and circularization is approximately exponential after that. The blue diamond symbols again indicate the formal beginning of the slow phase.

for  $e_c(0) \gtrsim 0.3$ ,  $e_c(\text{now}) \gtrsim 0.2$ ,  $a_c \gtrsim 0.35$  AU and  $m_c \gtrsim 0.05 M_J$ , and below  $v_* = 5 \text{ ms}^{-1}$  for  $e_c(0) \gtrsim 0.5$ ,  $e_c(\text{now}) \gtrsim 0.3$ ,  $a_c \gtrsim 0.4$  AU and  $m_c \gtrsim 0.05 M_J$ . However, notice the orange patches around  $a_c = 0.2$  AU corresponding to  $m_c < 0.03 M_J$ : enlargements of these are shown in Figure 12. The slow phase of the evolution of these systems actually involves an *increase* in  $e_p$  as discussed in Section 3.3.4, so that companion masses as low as  $1 M_\oplus$  are capable of exciting significant eccentricity in the observed planet. Some systems reach eccentricities around 0.02 (the aqua points in the top three plots of Figure 12). This effect is more pronounced when  $Q_p$  is higher as is demonstrated in Figure 13 for the case  $Q = 3 \times 10^5$ .

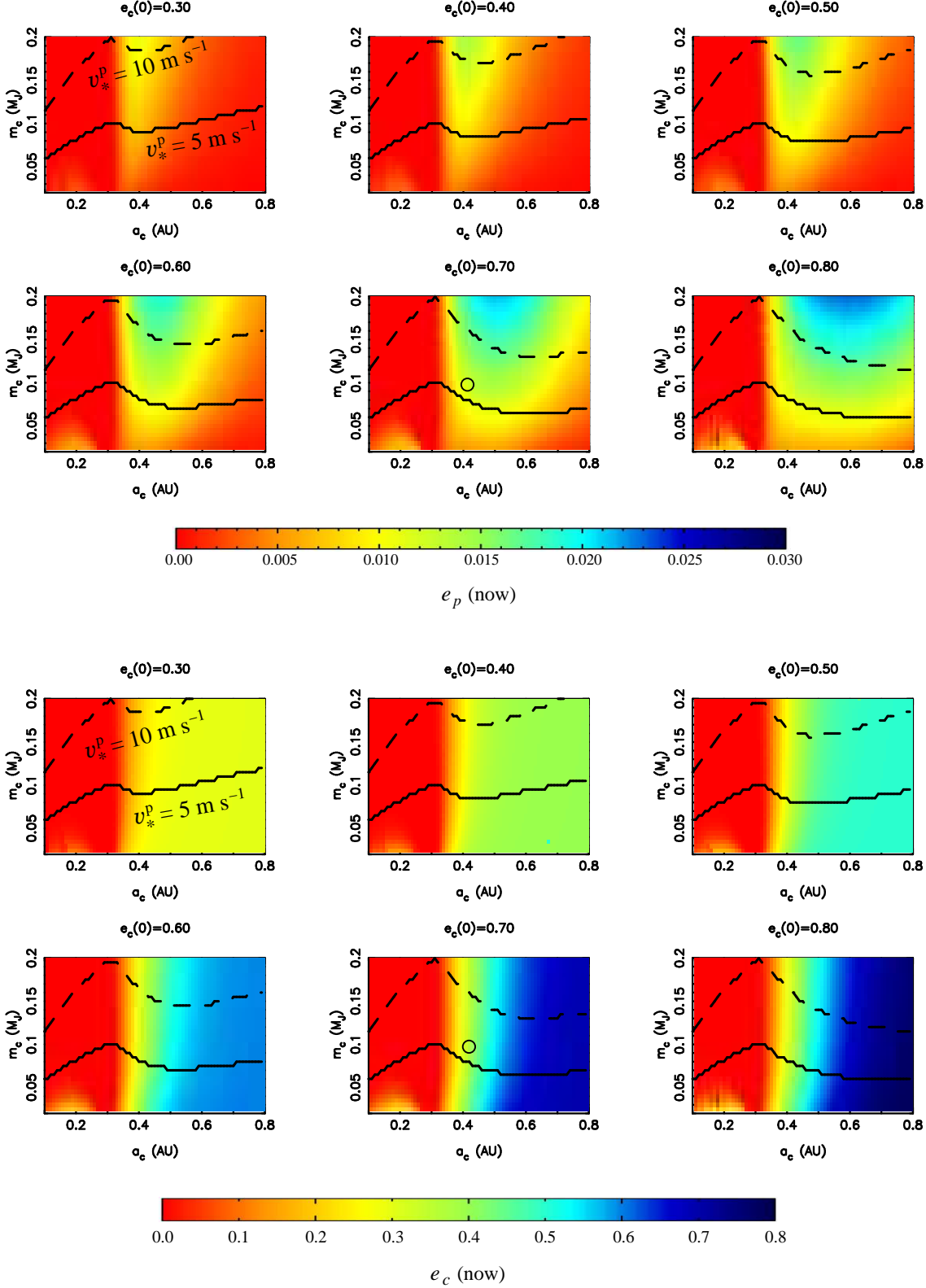
## 4.2 HAT-P1

HAT-P1 is a member of a binary system for which the projected separation of the stars is 1550 AU (Bakos et al. 2006). At this distance, the companion is incapable of inducing any eccentricity in the planet's orbit because the tidal damping timescale is far shorter than any timescale on which eccentricity could be induced.

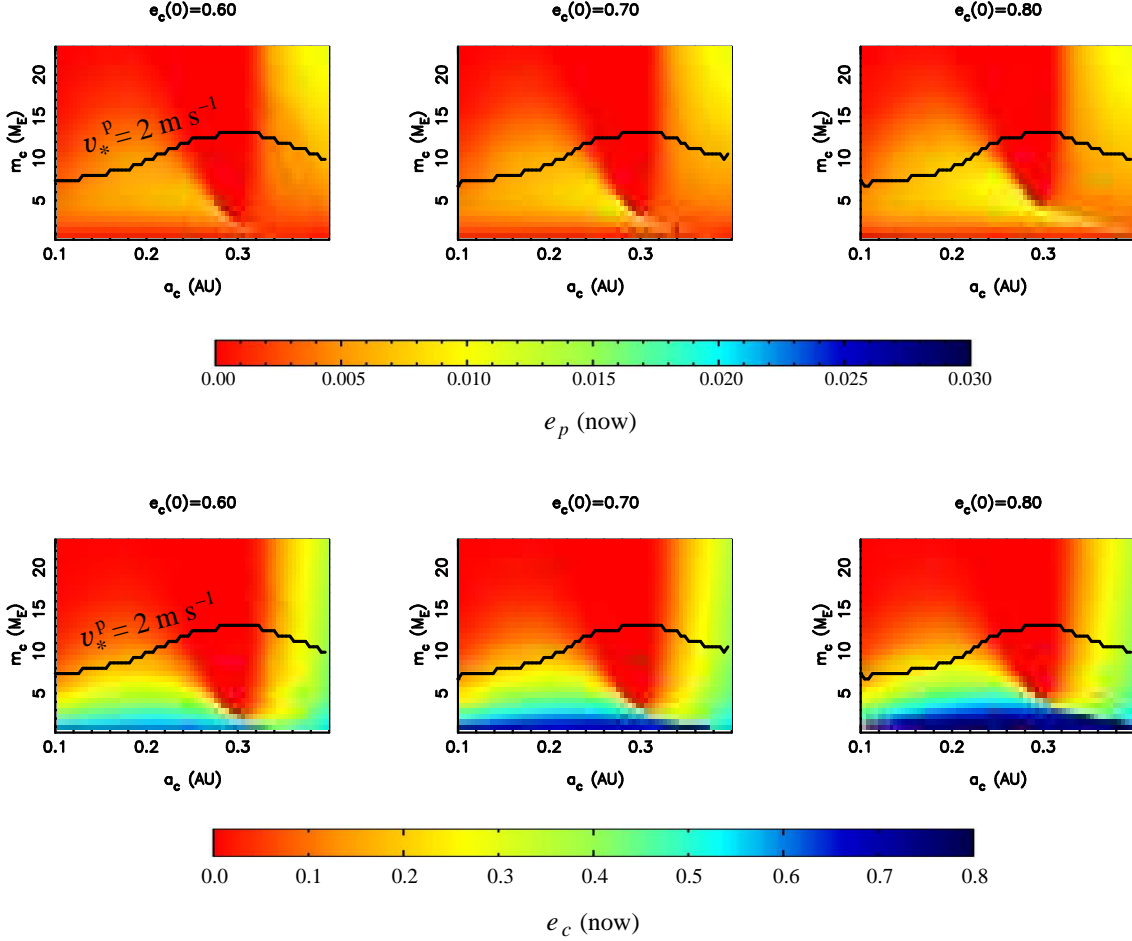
As far as the author is aware, at the time of writing no upper bound has been put on the reflex velocity of the star due to a companion planet. The preliminary value of  $e_p = 0.09 \pm 0.02$  awaits refinement, however, as Bakos et al. (2006) note, it produces a similar tidal dissipation rate in the planet to HD 209458b, consistent with its similar radius and its increased distance from the star (see Table 2). We have performed similar experiments for this system as was done for HD 209458,



HD 209458: age = 5.5 Gyr,  $Q_p = 10^5$



**Figure 11.** Current values of  $e_p$  (top six panels) and  $e_c$  (bottom six panels) for HD 209458b assuming an age for the system of 5.5 Gyr as well as  $Q_p = 10^5$ . Initial values for  $e_c$  are indicated at the top of each panel, while  $e_p(0) = 0.1$  and  $\eta(0) = 170^\circ$  for all experiments. The minimum companion mass is  $m_c = 0.02M_J = 6.67M_\oplus$ . Note the circle on the panels corresponding to  $e_c(0) = 0.7$ : although the companion orbit starts with a high eccentricity, its current eccentricity is relatively low (around 0.35). Also shown are curves of constant stellar reflex velocity,  $v_*^p$ , due to the companion *at periastron*. See text for discussion.

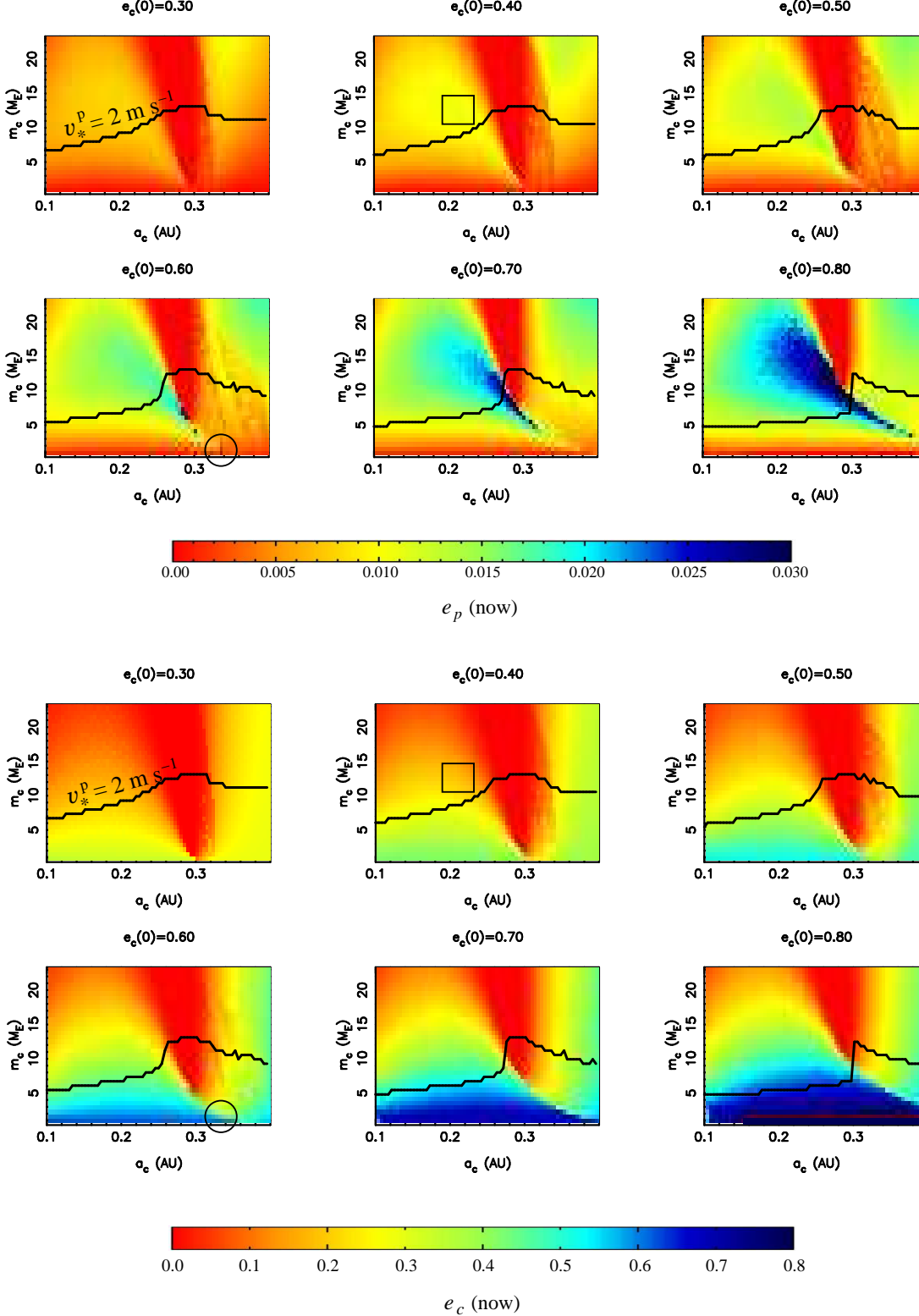
HD 209458: age = 5.5 Gyr,  $Q_p = 10^5$ 

**Figure 12.** Detail of some of the lower left-hand corners of the panels in Figure 11. These indicate that solutions exist even for companion masses as low as an Earth mass. Note in particular the blue dots in the top panels indicating relatively high eccentricities: these correspond to the maxima see in Figures 5 and 6. Note also that not all systems represented here would be stable had a direct integration code been used to do the integrations (Mardling & Lin 2004). The minimum companion mass is  $m_c = 0.001 M_J = 0.33 M_\oplus$ . Also shown are curves of constant stellar reflex velocity due to the companion *at periastron*.

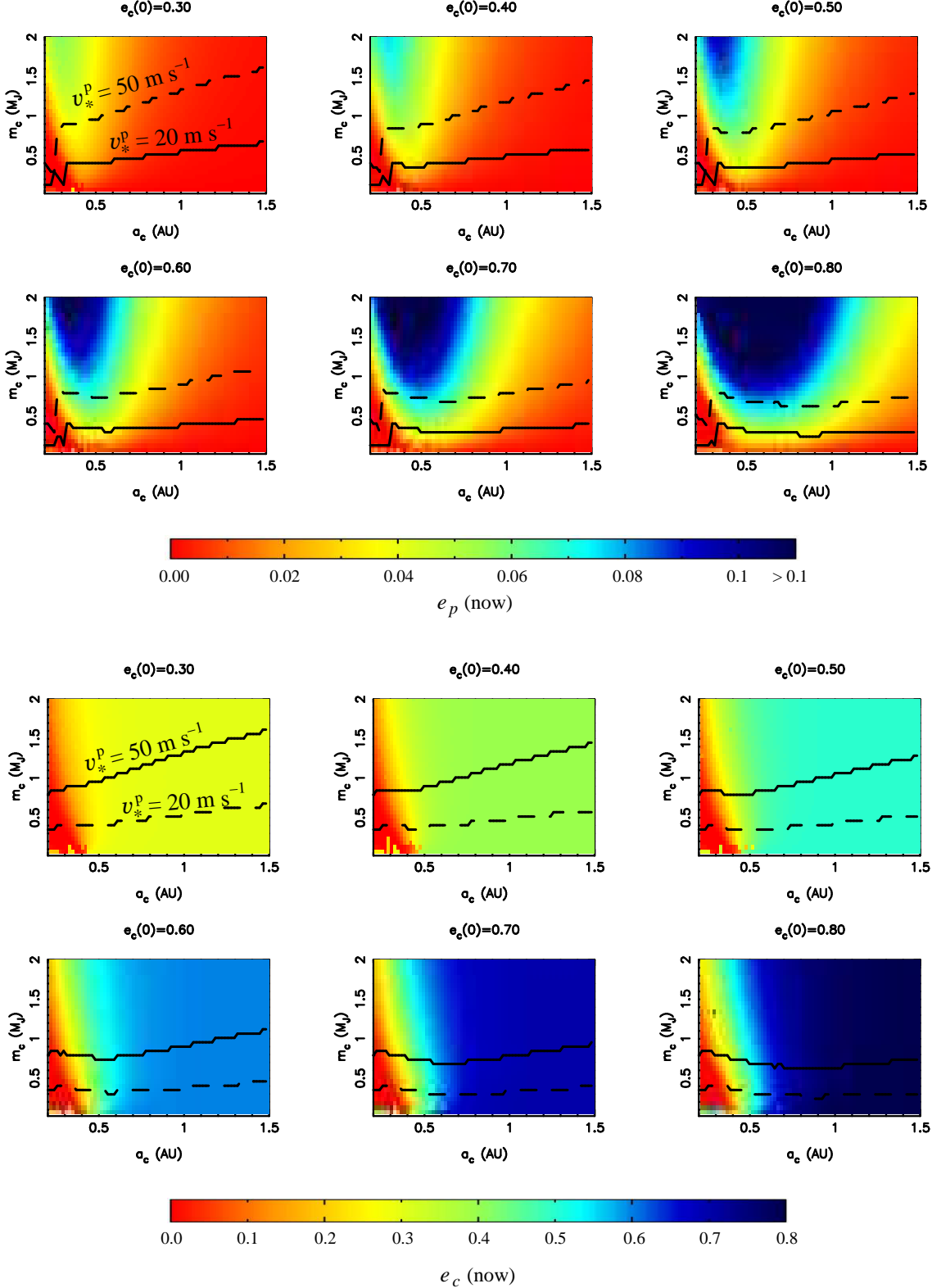
except for a wider range of companion masses and semimajor axes. The results of these are presented in Figures 14 and 15 for  $Q_p = 10^5$ , the latter focussing on the very low-mass regime. These results suggest that if a companion planet is responsible for the inflated radius of HAT-P1b, it should be detectable in the radial velocity signal, except if a very low-mass companion is responsible (Figure 15). If a companion planet is detected and a reliable measurement of the eccentricity of HAT-P1b is made (as well as reliable estimates for the companion’s mass, semimajor axis and eccentricity), it may be possible to use the theory developed here to deduce a relationship between the  $Q$ -value of HAT-P1b and  $e_c^*$ , and moreover, to put a lower bound on the value of  $Q_p$  (recall that  $e_c^*$  is the companion’s eccentricity when the system enters the slow phase and hence is an estimate of the initial eccentricity). The procedure is as follows.

(i) Check how accurately equation (36) giving the relationship between  $e_p$  and  $a_p$ ,  $a_c$ ,  $m_p$ ,  $m_c$  and  $e_c$  holds. Any substantial departure will be due to either (a) a nearby third planet; or (b) a significantly non-zero mutual inclination; or (c) a  $Q$ -value which is large enough for the system not to have yet entered the slow phase. In case (a), a third planet will modulate the eccentricity of its inner siblings, thereby preventing the equilibrating process from occurring (unless  $3\tau_c^{\text{true}}$  is less than the age of the system, in which case the process can work on all three planets!) In case (b), the effect of mutual inclination is shown in Figure 16. The value of  $e_c^*$  is slightly reduced, and the eccentricity is no longer non-oscillatory during the slow phase, although the oscillation amplitude is small for moderate mutual inclinations. The mutual inclination itself oscillates with an amplitude of around  $20^\circ$ . Inclinations need to be greater than around  $40^\circ$  to significantly affect the evolution. In

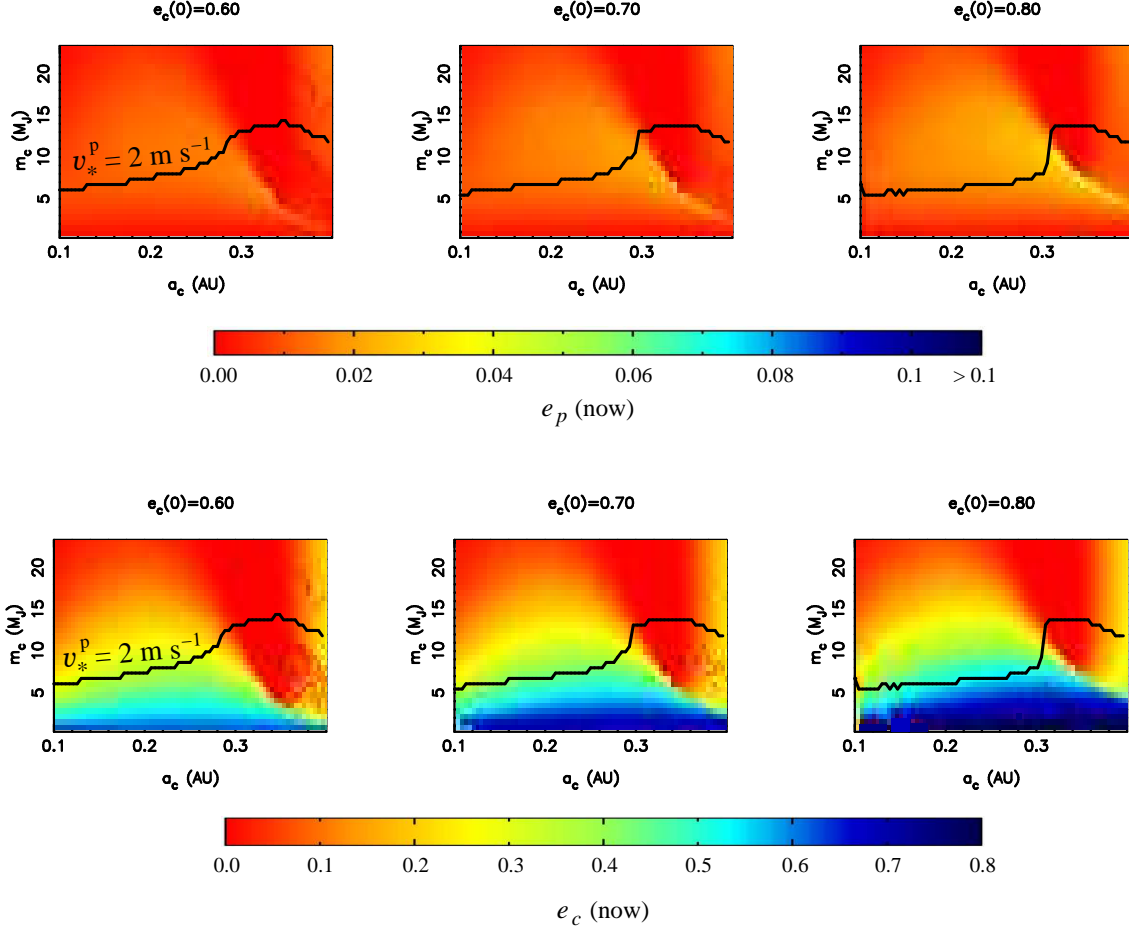
HD 209458: age = 5.5 Gyr,  $Q_p = 3 \times 10^5$



**Figure 13.** Similar to Figure 12 but with  $Q_p = 3 \times 10^5$  showing the dramatic effect increasing  $Q_p$  has on  $e_p(\text{now})$ . Note the general reduction in the values of  $e_c$  from  $e_c(0)$  to  $e_c(\text{now})$ . Example “solutions” are those in the square and the circle, the latter corresponding to a companion mass of  $0.97 M_\oplus$  with  $e_p(\text{now}) = 0.03$ ,  $e_c(\text{now}) = 0.46$  and  $a_c = 0.33$  AU. This solution is near a maximum; previous to this its average value was 0.006, that is, less than our definition of a “solution”. Solutions exist for  $e_c(0) \geq 0.4$ , an initial eccentricity not inconsistent with those found by Mandell, Raymond, & Sigurdsson (2007); higher values of  $e_c(0)$  yield more solutions. Also shown are curves of constant stellar reflex velocity due to the companion *at periastron*.

HAT-P1: age = 3.6 Gyr,  $Q_p = 10^5$ 

**Figure 14.** Current values of  $e_p$  (top six panels) and  $e_c$  (bottom six panels) for HAT-P1b assuming an age for the system of 3.6 Gyr as well as  $Q_p = 10^5$ . Initial values for  $e_c$  are indicated at the top of each panel, while  $e_p(0) = 0.1$  and  $\eta(0) = 170^\circ$  for all experiments. Note the scale used for  $e_p(\text{now})$  is different to that used for HD 209458. The tentative observed eccentricity is  $0.09 \pm 0.02$ . Also shown are curves of constant stellar reflex velocity due to the companion at periastron. See text for discussion.

HAT-P1: age = 3.6 Gyr,  $Q_p = 10^5$ 

**Figure 15.** Detail of lower-left-hand corner of Figure 14; note the scale used for  $e_p(\text{now})$  is different to that used for HD 209458. The tentative observed eccentricity is  $0.09 \pm 0.02$ . Compare Figure 12 with Figure 13 to get an idea of how this figure changes with increasing  $Q_p$ . Also shown are curves of constant stellar reflex velocity due to the companion at *periastron*.

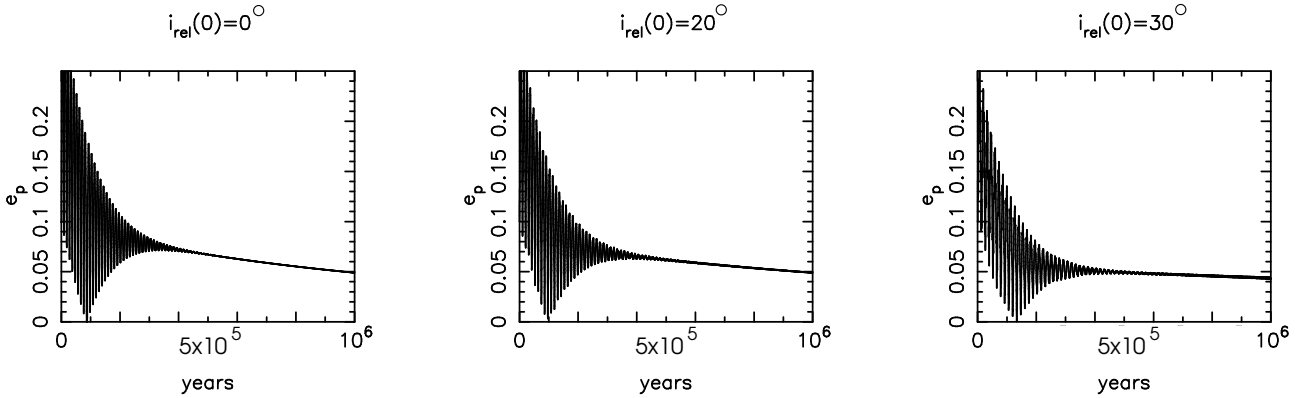


**Figure 16.** The effect of inclination. When the orbits are mutually inclined the value of  $e_c^*$  is reduced slightly, and the eccentricity is no longer non-oscillatory during the slow phase, although the oscillation amplitude is small for moderate mutual inclinations. This example is for a HAT-P1-type system with  $a_c(0) = 0.4$ ,  $e_c(0) = 0.5$ ,  $m_c = 0.5 M_J$  and  $Q_p$  again set artificially low at 100.

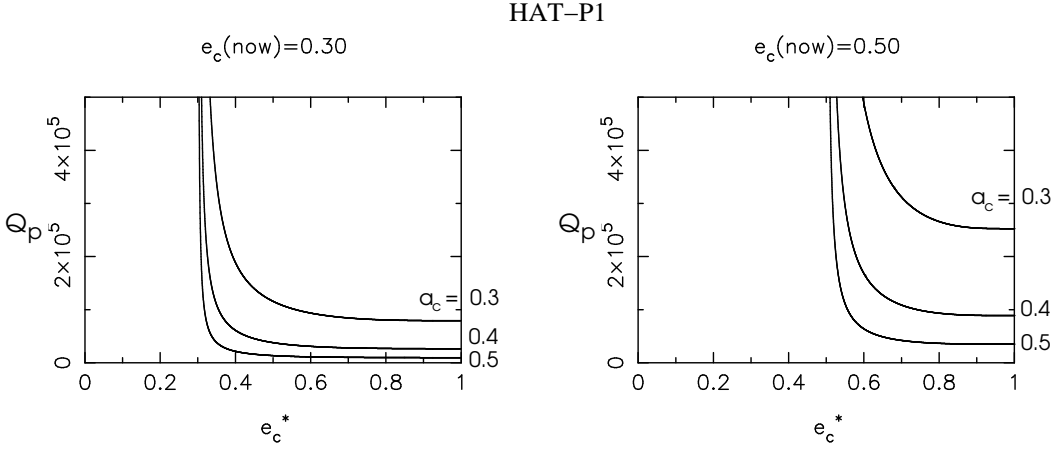


**Figure 17.** Using observed data to put a lower bound on  $Q_p$  for HAT-P1b. Example shown here is for  $m_c = 1M_J$ . See text for discussion.

case (c), since  $t_c \simeq 3\tau_{circ} \simeq 0.33$  Gyr for  $Q_p = 10^5$ ,  $Q_p$  would have to be greater than  $10^6$  to still be substantially far from pseudo-equilibrium (given an age of 3.6 Gyr).

(ii) Given that (36) is satisfied, (57) can be used with  $t = 3.6$  Gyr and  $t_c = 3\tau_{circ}$  to give a relationship between  $Q_p$  and  $e_c^*$  and in particular, to put a lower bound on  $Q_p$ . Examples of this are plotted in Figure 17 for  $m_c = 1M_J$  and for several values of  $a_c$  and  $e_c(\text{now})$ . For example, if a companion is found at  $a_c = 0.4\text{AU}$  with  $e_c = 0.5$  (corresponding to  $e_p = 0.11$ ), one can conclude that  $Q_p > 1.0 \times 10^5$ .

### 4.3 WASP-1

While Burrows et al. (2007) find that around four times as much energy is required to inflate WASP-1b to its observed size than for HD 209458b (they used a value for its mass of  $0.87M_J$ ; its revised estimate is  $0.79M_J$  compared to  $0.64M_J$  for HD 209458), its closer proximity to the parent star results in a similar value for  $e_p$  for both systems (see Table 1). While there is currently no published estimate for the eccentricity of WASP-1b, Figure 18 indicates values of  $e_p$  and  $e_c$  for a range of values of  $m_c$ ,  $a_c$  and  $e_c(0)$ , and for an estimated age of 2 Gyr. Table 2 suggests that  $e_p$  is likely to be similar to that of HD 209458 if a companion is responsible for its inflated radius, and Figure 18 presents plenty of solutions. Very low-mass solutions also exist for this system, albeit for a smaller range of parameters (or higher  $Q$ -values) than for HD 209458b and HAT-P1b.

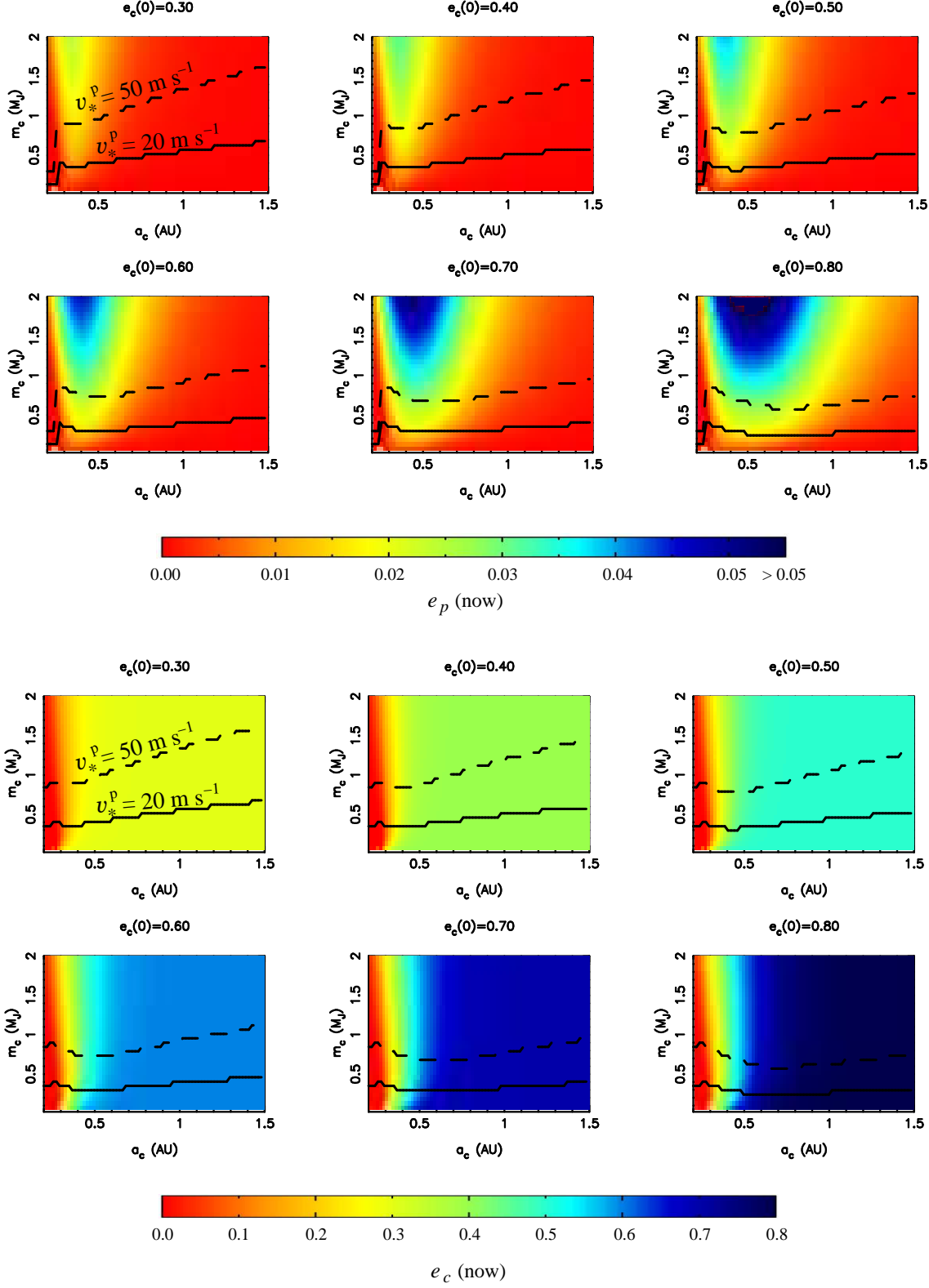
In contrast to HAT-P1, it almost certainly *will* be possible to put a lower bound on the value of  $Q_p$  if a companion planet is detected and a reliable measurement of the eccentricity of WASP-1b is made (as well as reliable estimates for the companion's mass, semimajor axis and eccentricity). This is because  $\tau_{circ}$  is only 14 Myr for  $Q_p = 10^5$ , so that  $Q_p$  would have to be greater than  $2.4 \times 10^6$  for the system to be substantially far from the equilibrium phase. Figure 19 is similar to Figure 17, however note the increase in  $Q_p$  for the case  $e_c(\text{now})=0.5$ ,  $a_c = 0.3\text{AU}$ . This is consistent with the fact that  $\tau_{circ}$  is relatively short, and since  $\tau_c^{true}$  (equation (60)) is proportional to  $\tau_{circ}$ , close companions will also circularize rather quickly unless  $Q_p$  is large.

## 5 CIRCULARIZING THE ORBITS OF PLANETS IN THE HABITABLE ZONE

Motivated by the work of Raymond, Mandell & Sigurdsson (2006), Mandell, Raymond, & Sigurdsson (2007) and Fogg & Nelson (2006) who find Earth-mass planets forming externally to a migrating gas giant after it scatters planetesimals outward past its own orbit, we use the analysis presented here to identify two-planet configurations for which the outer planet resides in the habitable zone of the system, and for which the circularization timescale of that planet would be longer than the age of the system without the assistance of a short-period companion. Using equation (57) with  $e_c = 0.02$  (it is singular at  $e_c = 0$ ), one can determine which values of  $m_c/m_p$  and  $a_c/a_p$  produce  $t < t_{age}$ , where  $t_{age}$  is the age of the star. Figure 20 shows an example of this for the case  $a_p = 0.04$ ,  $m_p = 0.6M_J$ ,  $e_c^* = 0.3$  and  $m_* = 0.6M_\odot$ . These parameters were chosen because the set of companion masses and semimajor axes for which the companion has already circularized contains a subset of Earth-mass planets which lie inside the habitable zone of the star, defined to be such that the semimajor axis lies in the range

$$0.8 (L_*/L_\odot)^{1/2} < a_c/\text{AU} < 1.5 (L_*/L_\odot)^{1/2}, \quad (62)$$

where  $L_*$  is the luminosity of the star and we have followed the definition given in Mandell, Raymond, & Sigurdsson (2007) which gives an empirical relationship (due to Scaledo) between the luminosity and the mass of a star. The habitable zone also

WASP-1: age = 2.0 Gyr,  $Q_p = 10^5$ 

**Figure 18.** Current values of  $e_p$  (top six panels) and  $e_c$  (bottom six panels) for WASP-1b assuming an age for the system of 2.0 Gyr as well as  $Q_p = 10^5$ . Initial values for  $e_c$  are indicated at the top of each panel, while  $e_p(0) = 0.1$  and  $\eta(0) = 170^\circ$  for all experiments. Note the scale used for  $e_p(\text{now})$  is different to that used for HD 209458 and the reflex velocity boundaries are  $v_* = 30 \text{ m s}^{-1}$  and  $v_* = 5 \text{ m s}^{-1}$ . There is currently no published estimate for  $e_p$ , however, Table 2 indicates that it is likely to be similar to that of HD 209458 if a companion is responsible for its inflated radius.

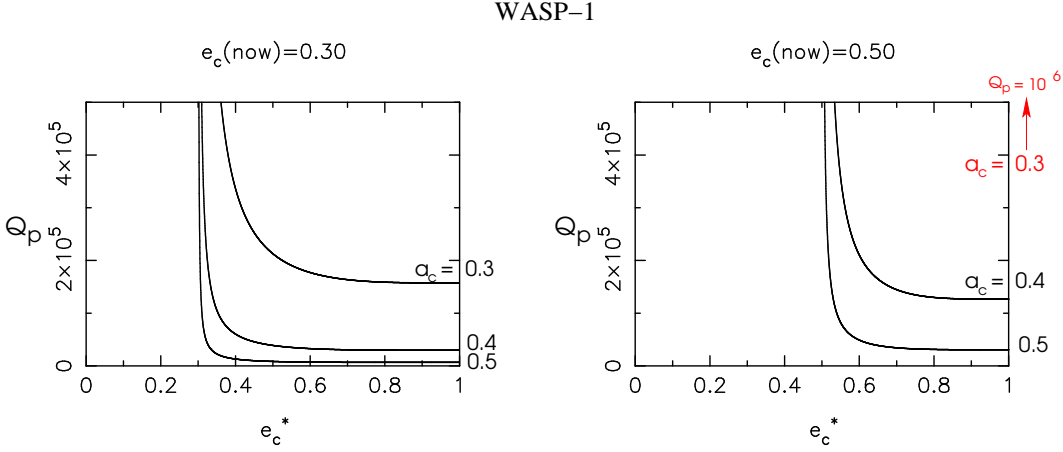


**Figure 19.** Using observed data to put a lower bound on  $Q_p$  for WASP-1b. Example shown here is for  $m_c = 1M_J$ . See text for discussion.

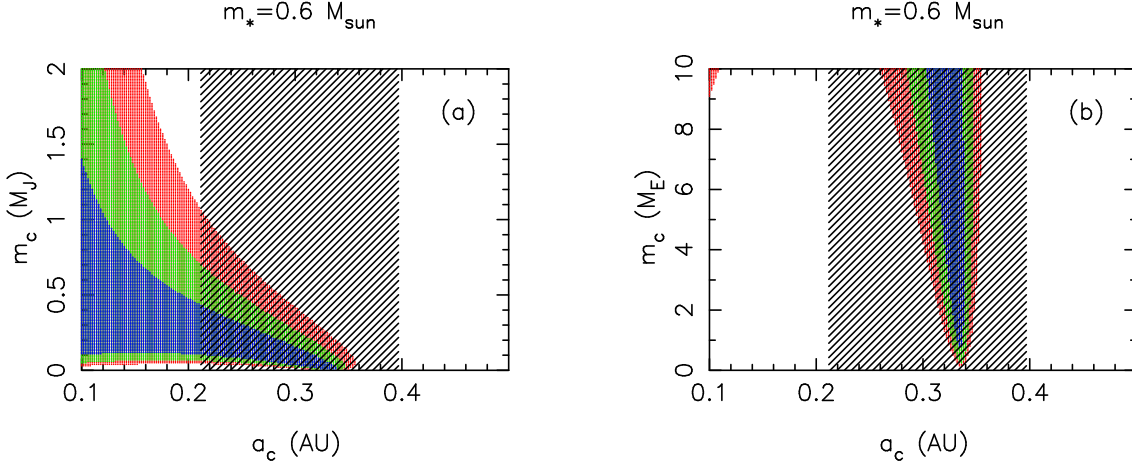


**Figure 20.** Circularized planets in the habitable zone. If the condition  $t < t_{age}$  is met, a coloured dot is plotted according to the scheme: red for  $t_{age} = 6$  Gyr, green for  $t_{age} = 3$  Gyr, and blue for  $t_{age} = 1$  Gyr. A  $Q$ -value of  $10^5$  and a radius of  $1.3R_J$  are assumed for the short-period planet. The hatched region corresponds to the habitable zone of the star. For these systems,  $a_p = 0.04$ ,  $m_p = 0.6M_J$ ,  $e_c^* = 0.3$  and  $m_* = 0.6M_\odot$ . Panel (b) shows detail of panel (a) for low-mass planets ( $M_E$  is the mass of the Earth).

contains a substantial fraction of planets with masses up to  $1M_J$ ; these systems are also of interest because they can harbour moons which could be habitable. Figure 21 shows the effect of decreasing and increasing the stellar mass. Increasing  $e_c^*$  pushes the minimum of the circularized region upwards; increasing the mass of the short-period planet pushes this region to the right as does increasing  $a_p$ .

Currently, there are no known isolated short-period pairs of planets to which this theory can be applied. However, low-mass stars are now being targeted more frequently so it seems likely such systems will be discovered in the near future.

## 6 SUMMARY AND DISCUSSION

### 6.1 Summary

The ideas and results presented in this paper are summarized as follows:

(i) If a planet is inflated because it is tidally heated, its radius is related to the orbital eccentricity by equation (3). The biggest uncertainties are the  $Q$ -value of the planet,  $Q_p$ , and the heating needed to maintain the planet's size,  $\mathcal{L}_p$ . The latter depends on the structural model used, and in particular, where inside the planet the energy is dissipated.

(ii) Conditions for libration and circulation of  $\eta = \varpi_p - \varpi_c$  including relativistic effects are given by (37) and (38) for the case that  $e_p \ll e_c$  and  $m_p \ll m_*$  (there are no conditions on  $m_c$ ), with the time dependence of  $e_p$ ,  $e_c$  and  $\eta$  given by (19), (26), (29), (17), (21), and (25), with  $e_p^{(eq)}$  given by (36).

(iii) The system evolves through three stages when tidal dissipation is present (Figure 3): (1) circulation of the angle



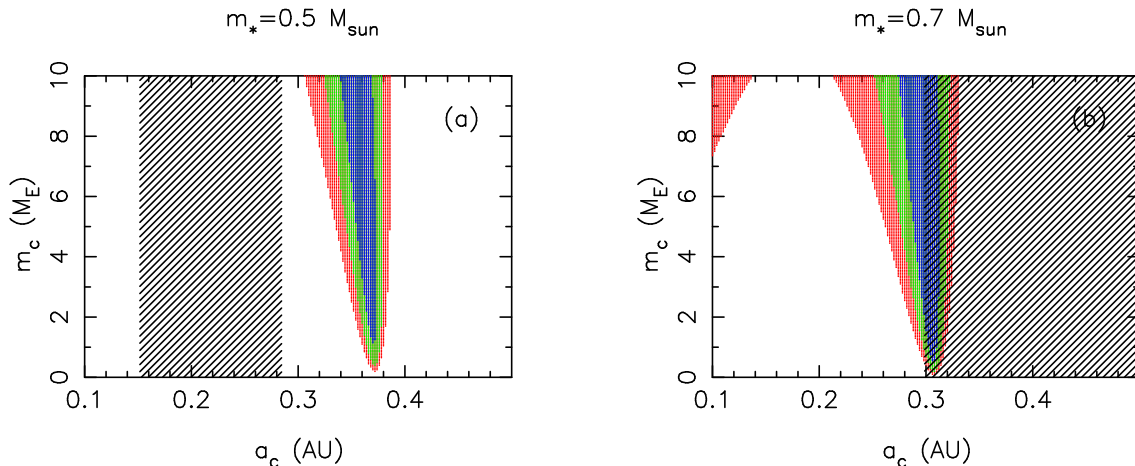


**Figure 21.** Same parameters as in Figure 20 but with (a)  $m_* = 0.5M_\odot$  and (b)  $m_* = 0.7M_\odot$ .

between the lines of apsides of the two planets accompanied by the slow oscillation of the eccentricities at *constant amplitude*, together with decline of the *mean* value of the inner planet's eccentricity until it reaches a (quasi)-fixed value (equation (45)): this occurs on the circularization timescale; (2) libration of the angle between the lines of apsides accompanied by the slow oscillation of the eccentricities with reducing amplitude but maintenance of the mean value of the inner eccentricity (equations (49) and (50) with the mean value  $e_p^{(eq)}$  given by (36)): this occurs on *twice* the circularization timescale; and (3) either (a): a slow non-oscillatory decline in both eccentricities to zero or (b): approximate maintenance of the inner eccentricity at the constant value  $e_p = e_p^*$  for some (often extremely long) period of time followed by its *increase* to some maximum value followed by an often fast decline of both eccentricities to zero. Both are described by (36) together with (57). Whether or not the final phase occurs via route (a) or (b), it proceeds on a timescale sometimes several orders of magnitude longer than the tidal circularization timescale of the inner planet,  $\tau_{circ}$ .

(iv) As a consequence of the existence of route (b) above, very low-mass companions are sometimes capable of sustaining the eccentricity needed to inflate short-period gas giants (eg. Figures 5 and 6). For this to occur it is at least necessary that the companion eccentricities are sufficiently high; the lower the companion mass the higher the initial eccentricity needed. The timescale on which the eccentricity is sustained increases with *decreasing* companion mass, however, the value of the sustained eccentricity decreases with decreasing mass. For a given system age, more solutions exist for higher values of  $Q_p$ . This scenario is supported by the work of Fogg & Nelson (2006) and Mandell, Raymond, & Sigurdsson (2007) (see discussion below).

(v) As well as the very low-mass solutions produced by route (b), route (a) produces solutions for which the eccentricity and hence radius of HD 209458b is sustained by a companion which produces a stellar reflex velocity below the stellar jitter estimate (Figure 11). More solutions exist for higher  $Q$ -values of HD 209458b.

(vi) Companion planet solutions are presented for HAT-P1 and WASP-1 for a wide range of companion parameters.

(vii) If companions to HAT-P1b and/or WASP-1b (or other systems like these) are discovered and reliable estimates of the system parameters can be made (and there is no sign of any other companions), it should be possible to put lower bounds on the  $Q$ -value of the short-period planet in the system (Figures 17 and 19). Moderately inclined orbits have little effect on the long-term evolution.

(viii) Long after the protoplanetary disk has disappeared, it is possible to circularize the orbits of some planets whose tidal circularization timescales are longer than the age of the system if they have short-period companions whose own values of  $\tau_{circ}$  are short. The circularization timescale of a companion is given by equation (60), and depends on the structure of the short-period planet.

(ix) In the light of work by Mandell, Raymond, & Sigurdsson (2007) and Fogg & Nelson (2006), systems with hot Jupiters orbiting stars with masses around  $0.5 - 0.7M_\odot$  are good candidates for finding *circular* Earth-mass planets in the habitable zone, as long as there is no third planet nearby.

## 6.2 Discussion

How much the early evolution of short-period two-planet systems proceeds according to the simple picture described here depends on how planets come to be in their current positions. If a gaseous disk pilots them in (Lin, Bodenheimer & Richardson 1996) it will influence this phase at some level, especially in a case like WASP-1b for which  $\tau_{circ}$  is as low as 14 Myr (a time comparable to the disk lifetime). If, instead, a planet is *scattered* in to its current position (Rasio & Ford 1996) it is likely

to arrive with significant eccentricity which must subsequently be damped. Recall that the analysis here assumes  $e_p \ll e_c$ , although relaxing this condition makes little difference to the overall picture.

In addition, conditions at the time of arrival will be very different to those in a mature system. For example, a planet's radius will be significantly larger, thereby increasing the strength of the tidal interaction with the star (see Fig. 1 in Bodenheimer, Lin & Mardling 2001 for the time-dependence of the planetary radius for several models). The stellar spin rate will be significantly higher, and in some cases be high enough to force an *increase* in the planet's eccentricity. The latter may account for the range of eccentricities observed in the "borderline planets" with periods in the range 7-21 days (Dobbs-Dixon, Lin & Mardling 2004).

It seems likely that Nature uses a hybrid of migration and scattering, thereby producing a rich variety of possible configurations (Moorhead & Adams 2005; Fogg & Nelson 2006; Mandell, Raymond, & Sigurdsson 2007; Nagasawa, Lin & Thommes 2005; Zhou et al. 2005). Of particular interest here is the situation where planetesimals are shepherded in by a migrating gas giant, these going on either to accumulate to form a hot Earth internal to the gas giant's orbit, or to be scattered out before accumulating in an external orbit (Mandell, Raymond, & Sigurdsson 2007; Fogg & Nelson 2006). In the former case the hot Earth is often subsequently scattered out, so that both scenarios produce eccentric low-mass objects with periods a few times that of the massive planet. The final eccentricities of these Earth-mass planets tend to be fairly low due to gas drag and dynamical friction with nearby planetesimals, however the simulations of the above authors sampled only a small range of initial conditions and it may be that substantially higher eccentricities can result from this process. The maximum eccentricity found by Mandell, Raymond, & Sigurdsson (2007) was 0.46 for a planet with mass  $0.32M_\oplus$  at  $a_c = 1.74$  AU outside a Jupiter-mass giant at  $a_p = 0.14$  AU (simulation JD-3 in their Table 4). Higher eccentricities may result when low-mass planets are scattered in via encounters with bodies further out in the disk. Note that the semimajor axis ratio in the above example was 12.4, about twice that of the Earth-mass "solutions" for HD 209458 (Figure 13), while others were substantially lower.

While extremely low-mass solutions are relatively improbable, Figure 13 indicates that there are many low-mass solutions for HD 209458 which are consistent with the findings of Fogg & Nelson (2006) and Mandell, Raymond, & Sigurdsson (2007), especially for such  $Q$ -values ( $3 \times 10^5$ ). While the findings of Bodenheimer, Laughlin & Lin (2003) and Burrows et al. (2007) suggest that only low  $Q$ -values are consistent with the observed eccentricity (if, indeed, it is non-zero), it should be remembered that these authors distributed the tidal energy homogeneously throughout the planet's envelope and implicitly assumed that the energy was dissipated locally. If, in reality, the energy is dissipated near the surface (but not so close to the surface that there is essentially no structural change (Wu 2005)), then less tidal energy may be needed to produce the observed radius for a given  $Q$ -value. This allows for higher  $Q$ -values to be associated with a given value of  $e_p$  so that solutions such as those shown in Figure 13 may, in fact, be viable. *If so, inflated planets are good targets in the search for terrestrial planets.*

Of course, while very low mass solutions are of extreme interest (and completely unexpected!), there are still many higher companion mass solutions for HD 209458b, especially for  $Q$ -values above  $10^5$ . While WASP-1b and HAT-P1b remain unconstrained (except for the latter's eccentricity), there exist almost unlimited potential solutions all of which offer the opportunity to put lower bounds on their  $Q$ -values if companion planets are discovered. Moreover, if companions are identified and their orbital parameters accurately measured, the analysis presented here can be used to constrain their history, in particular, their "initial" eccentricity.

Conclusions such as these are possible as long as there is no third planet nearby, and as long as one is confident that the circularization timescale (or more precisely, *three times* the circularization timescale) is shorter than the age of the system. Another possible departure from the assumptions made in this analysis is non-coplanarity. However, unless the relative inclination of the two planets is substantial, say, greater, than around  $40^\circ$ , non-coplanarity makes very little difference to the predicted outcome, as has been verified by integration of the full secular equations (Figure 16).

Remarkably, at this stage there are no known two-planet systems for which the innermost planet has a circularization timescale less than a Gyr, and thus it is currently not possible to compare our two-planet model with a real system. In the meantime, equations (36) and (58) provide clear guidance on how such systems depend on the system parameters.

## ACKNOWLEDGMENTS

The author wishes to thank Doug Lin for valuable discussions and support.

## REFERENCES

- Adams, F. C. & Laughlin, G. 2006, ApJ, 649, 992
- Adams, F. C. & Laughlin, G. 2006, ApJ, 649, 1004
- Agol, E., & Steffen, J. H., MNRAS, 374, 941
- Arras, P., & Bildsten, L. 2006, ApJ, 650, 394

- Bakos, G. A. et al. 2007, ApJ 656, 552
- Banfield, D., & Murray, N. 1992, Icarus, 99, 390
- Bodenheimer, P., Laughlin, G., & Lin, D. N. C. 2003, ApJ, 592, 555
- Bodenheimer, P., Lin, D. N. C. & Mardling, R. A. 2001, ApJ, 548, 466
- Bodenheimer, P., & Pollack, J. B. 1986, Icarus, 67, 391
- Boss, A. P. 1997, Science, 276, 1836
- Burrows, A., Guillot, T., Hubbard, W. B., Marley, M. S., Saumon, D., Lunine, J. I., & Sudarsky, D. 2000, ApJL, 534, 97
- Burrows, A., Hubeny, I., Budaj, J., & Hubbard, W. B. 2007, ApJ, 661, 502
- Burrows, A., Sudarsky, D., & Hubbard, W. B. 2003, ApJ, 594, 545
- Cameron, A. G. W. 1978, Moon Planets, 18, 5
- Charbonneau, D., Brown, T. M., Latham, D. W., & Mayor, M. 2000, ApJL, 529, 45
- Charbonneau, D., Brown, T. M., Noyes, R. W., & Gilliland, R. L. 2002, ApJ, 568, 377
- Collier Cameron A. et al. 2006, astro-ph/0609688
- Charbonneau, D., Brown, T. M., Latham, D. W., & Mayor, M. 2000, ApJL, 529, 45
- Croll, B., et al. 2007, ApJ, 658, 1328
- Deming, D., Seager, S., Richardson, L. J., & Harrington, J. 2005, Nature, 434, 740
- Dobbs-Dixon, I., Lin, D. N. C., & Mardling, R. A. 2004, ApJ, 610, 464
- Fabrycky, D. C., Johnson, E. T., & Goodman, J. 2007, astro-ph/0703418
- Fogg, M. J., & Nelson, R. P. 2007, A&A, 461, 1195
- Ford, E. B., Kozinsky, B., & Rasio, F. A. 2000, ApJ, 535, 385
- Fortney, J. J., Marley, M. S., & Barnes, J. W. 2007, ApJ, 659, 1661
- Goldreich, P., & Soter, S. 1966, Icarus, 5, 375
- Guillot, T., & Showman, A. P. 2002, A&A, 385, 156
- Henry, G. W., Marcy, G. W., Butler, R. P., & Vogt, S. S. 2000, ApJL, 529, 41
- Knutson H., Charbonneau D., Noyes R. W., Brown T. M., Gilliland R. L. 2007, ApJ 655, 564
- Kuiper, G. P. 1951, in Astrophysics, ed. J. Hynek (New York: McGraw Hill), 357
- Laughlin, G., Marcy, G. W., Vogt, S. S., Fischer, D. A., & Butler, R. P. 2005, ApJ, 629, L121
- Lee, M. H., & Peale, S. J. 2003, ApJ, 592, 1201
- Lin, D. N. C., Bodenheimer, P., & Richardson, D. C. 1996, Nature, 380, 606
- Mandell, A. M., Raymond, S. N., & Sigurdsson, S. 2007, ApJ, 660, 823
- Mardling, R. A. 2007a, *in preparation*
- Mardling, R. A. 2007b, *in preparation*
- Mardling, R. A., & Lin, D. N. C. 2002, ApJ, 573, 829
- Mardling, R. A., & Lin, D. N. C. 2004, ApJ, 614, 955
- Moorhead, A. V., & Adams, F. C. 2005, Icarus, 178, 517
- Murray, C. D., & Dermott, S. F. 2000, Solar System Dynamics, by C.D. Murray and S.F. Dermott., Cambridge, UK: Cambridge University Press
- Nagasawa, M., Lin, D. N. C., & Ida, S. 2003, ApJ, 586, 1374
- Nagasawa, M., Lin, D. N. C., & Thommes, E. 2005, ApJ, 635, 578
- Ogilvie, G. I., & Lin, D. N. C. 2004, ApJ, 610, 477
- Rasio, F. A., & Ford, E. B. 1996, Science, 274, 954
- Rasio, F. A., Tout, C. A., Lubow, S. H., & Livio, M. 1996, ApJ, 470, 1187
- Raymond, S. N., Mandell, A. M., & Sigurdsson, S. 2006, Science, 313, 1413
- Safronov, V. S. 1969, Evolution of the Protoplanetary Cloud and Formation of the Earth and Planets (Moscow: Nauka)
- Stempels, H. C., Collier Cameron, A., Hebb, L., Smalley, B., & Frandsen, S. 2007, arXiv:0705.1677
- Tittlemore, W. C., & Wisdom, J. 1989, Icarus, 78, 63
- Wetherill, G. W. 1980, ARA&A, 18, 77
- Winn, J. N., & Holman, M. J. 2005, ApJL, 628, 159
- Wu, Y. 2003, in ASP Conf. Ser. 294, Scientific Frontiers in Research on Extrasolar Planets, ed. D. Deming & S. Seager (San Francisco: ASP), 213
- Wu, Y. 2005, ApJ, 635, 688
- Yoder, C. F., & Peale, S. J. 1981, Icarus, 47, 1
- Zhou, J.-L., Aarseth, S. J., Lin, D. N. C., & Nagasawa, M. 2005, ApJL, 631, L85